Investigation of Secondary (Dean) Flows in Curved Microchannels and Application to Microparticle Sample Preparation

Pouriya Bayat

A THESIS SUBMITTED TO THE
FACULTY OF GRADUATE STUDIES
IN PARTIAL FULFILLMENT OF THE REQUIREMENTS
FOR THE DEGREE OF
MASTER OF APPLIED SCIENCE

Graduate Program in
MECHANICAL ENGINEERING
York University
Toronto, Ontario
August 2017

Abstract

Exchanging the solution of microparticles from a complex source fluid to a target clean buffer is important for sample preparation in portable microfluidic and point-of-care diagnostic devices. Current portable solution exchange methods are often limited in throughput or have low efficiencies. In this thesis, a novel method involving inertial focusing of microparticles at the inner wall of a curved channel and secondary Dean flow-based exchange of their fluid is investigated. The fluid behavior in curved microchannels is thoroughly studied and the effects of radius of curvature, hydraulic diameter, width and height of the channel and viscosity of the fluid on the development of Dean vortices are investigated experimentally and numerically. A comprehensive correlation for estimating the average lateral Dean velocity of the fluid is also proposed. The outcomes of the fluidic study is then combined with inertial particle focusing to devise a microfluidic platform for exchanging the solution of 11 µm and 19 µm microparticles. This was achieved with an unprecedented flow rate of 1 $mL.min^{-1}$ and throughput of 10^4 $particle.s^{-1}$ at high efficiencies. Additionally, the application of the device for isolation of cell surrogates from a bacterial solution is shown. This technology can be used as a portable micro-centrifuge for sample preparation in point-of-care devices.

Acknowledgment

I would like to express my gratitude to my supervisor Dr. Pouya Rezai for his continuous support throughout my studies. It was impossible to take this journey without his guidance and constructive advice. It was a blessing to be able to improve my personality while I had the freedom to enjoy thinking creatively under his supervision. In Acute, I had the chance to not only improve my abilities as an independent researcher but also gain valuable writing, presentation and management skills. A part of me will always be with the Acute Lab.

I am also thankful to Dr. Alidad Amirfazli and Dr. Magdalena Krol who showed interest in my research and kindly accepted examining my thesis.

I would love to express my sincere love and gratitude to my wife who has always been there for me. I will forever be indebted to her for all her love, patience and kind support. Thank you for making my life brighter than ever. The biggest dreams are achievable with you.

My parents, my brother and my aunt deserve the greatest appreciations for being the ones who never stopped believing in me. The world is a lovely place with you.

Finally, I would love to dedicate my thesis to my grandfather for whom I always remained “the Doctor”. May he rest in peace.

Table of Contents

List of Figures

300MM×150MM BOTH WITH R=1 CM) WERE USED IN OUR STUDIES.

FIGURE 2-3. NUMERICAL MODEL USED FOR DETERMINATION OF DEAN VELOCITY. (A) GEOMETRY OF A MICROCHANNEL WITH R=0.5 CM AND CROSS-SECTIONAL DIMENSION OF 150µM×150µM. (B) MESH ELEMENTS IN THE REGION OF INTEREST (ROI) SHOWN IN (A). THE NUMBER OF MESH ELEMENTS INCREASED AT THE WALL. TOTAL NUMBER OF ELEMENTS WERE APPROXIMATELY 8×10^5. (C) VELOCITY DISTRIBUTION OVER YZ-PLANES FOR WATER AT DE=12. (D) PRESSURE CONTOURS FOR THE GEOMETRY PRESENTED IN (A) AND THE FLOW CONDITIONS MENTIONED IN (C).

FIGURE 2-4. CO-FLOW IMAGES OF METHYLENE BLUE (MB) AND WATER AT INLET FLOW RATE OF 0.6 $ML.MIN^{-1}$ (I.E., VELOCITY OF 0.22 $M.S^{-1}$) ALONG THE LENGTH OF A 300µM×150µM CURVED MICROCHANNEL WITH R=1CM (A-1 TO A-4) AND INTENSITY DIAGRAMS CORRESPONDING TO ASSESSMENT LINES AB ALONG THE WIDTH OF THE CHANNEL AT SPECIFIC CONTROL POINTS IN EACH IMAGE (B-1 TO B-4). (A-1 AND B-1) SHOW THE BEGINNING OF THE CHANNEL WHERE THE INTENSITY DIAGRAM WAS SIMILAR TO A STEP FUNCTION AND THE FLUIDS WERE COMPLETELY SEPARATED, I.E., WATER AT INNER WALL (IW) AND MB AT OUTER WALL (OW). IN (A-2 AND B-2), MB AND WATER STARTED TO DISPLACE LATERALLY DUE TO DEAN FLOW VORTICES. IN (A-3 AND B-3), WATER WAS COMPLETELY SANDWICHED IN BETWEEN MB LAYERS, AND THE INTENSITY DIAGRAM WAS ALMOST UNIFORM. IN (A-4 AND B-4), WATER AND MB STARTED TO APPEAR CLOSER TO THE OW AND IW, RESPECTIVELY, HENCE DEMONSTRATING SWITCHING IN POSITION COMPARED TO THEIR INITIAL CONDITIONS.

FIGURE 2-5. SWITCHING INDEX (SI) DIAGRAMS ALONG THE LENGTH OF THE CHANNEL AT

VARIOUS INLET AXIAL VELOCITIES, V_X, OF METHYLENE BLUE AND WATER THAT WERE CO-INJECTED INTO A DEVICE WITH R=2 CM AND CROSS SECTION AREA OF 150µM×150µM. SI DECREASES ALONG THE CHANNEL AS THE TWO SOLUTIONS FORM COUNTER-ROTATING VORTICES AND INCREASES WHEN THEY START SEPARATING FROM EACH OTHER INTO DISTINCT PHASES AGAIN DOWNSTREAM THE CHANNEL. THE FIRST PEAK IN THE SI PLOT INDICATES THE EXACT LOCATION OF THE FIRST SWITCH IN POSITION (L_S) OF METHYLENE BLUE AND WATER SOLUTIONS (I.E., 180º RECIRCULATION). AT HIGHER AXIAL VELOCITIES, A SECOND SWITCH CORRESPONDING TO A FULL 360º RECIRCULATION OF FLUIDS CAN BE CLEARLY SEEN. ERROR BARS REPRESENT THE STANDARD DEVIATION OF THREE EXPERIMENTAL REPEATS.

FIGURE 2-6. DEAN VORTEX SHAPE APPROXIMATION AND CALCULATED AVERAGE DEAN VELOCITIES IN A CURVED MICROCHANNEL WITH R=2 CM AND CROSS SECTION AREA OF 150µM×150µM. DEAN VORTICES WERE ASSUMED TO FOLLOW (A) AN ELLIPTICAL PATH FOR Δ<0.008 ($\Delta = \mathrm{D}/2\mathrm{R}$) AND (B) A HALF-ELLIPTICAL HALF-CIRCULAR PATH FOR $\Delta >$0.008[34]. (C) THE SWITCHING LENGTHS OBTAINED EXPERIMENTALLY AND THE APPROXIMATED AVERAGE LATERAL TRAVEL DISTANCES WERE USED TO CALCULATE THE AVERAGE DEAN VELOCITIES (V_{DE}) AT DIFFERENT AXIAL VELOCITIES IN THE ABOVEMENTIONED DEVICE. THE SOLID LINE IN (C) SHOWS A POWER FUNCTION ($V_{DE}=ADE^B$) FITTED OVER THE EXPERIMENTAL DATA POINTS WITH CONSTANTS A=0.072 AND B=2 (R^2=0.98). THE DASHED LINE IN (C) SHOWS THE OOKAWARA'S[67] EQUATION FOR DEAN VELOCITY (MM.S^{-1}) WITH A=0.18 AND B=1.63 (R^2= 0.71).

FIGURE 2-7. EFFECT OF RADIUS OF CURVATURE OF THE CHANNEL (R=0.5-2CM) ON DEAN

CURVED MICROCHANNEL WITH R=0.5 CM SHOWN (A) AT VARIOUS AXIAL VELOCITIES AND (B) USING THE NON-DIMENSIONAL DEAN NUMBER. INCREASING THE VISCOSITY WHILE AXIAL VELOCITY IS CONSTANT CAUSED A REDUCTION IN V_{DE}. HOWEVER, WHEN DEAN NUMBER WAS KEPT CONSTANT, VISCOSITY DIRECTLY AFFECTED THE V_{DE}. SINGLE A AND B CONSTANTS COULD NOT BE FOUND TO PREDICT V_{DE} WITH A SINGLE POWER FUNCTION ($V_{DE}=ADE^{B}$).

FIGURE 2-11. DEAN VELOCITY PLOTTED AGAINST NSNDEB BASED ON ALL NUMERICAL AND EXPERIMENTAL RESULTS OBTAINED IN THIS STUDY. (A-C)THE MAGNITUDE OF B WAS SET TO 1.63 FOR SIMILARITY IN DE POWER TO THE COMMONLY USED VALUE IN THE LITERATURE WHILE N WAS VARIED FROM 0.25 TO 2.5 TO OBTAIN THE BEST FIT (I.E. N=1). (D-F) SUPERIORITY OF B=1.63 WAS TESTED BY SETTING N=1 (CONCLUDED FROM A-C) AND CHANGING B FROM 0.25 TO 2.5

FIGURE 2-12. VALUES OF R^2 FOR (A) CONSTANT N AND B AS THE VARIABLE AND (B) CONSTANT B AND VARIABLE N. THE MAXIMUM VALUE FOR R^2 IS SEEN FOR THE CASE OF N=1 AND B=1.63.

FIGURE 2-13. DEAN VELOCITY PLOTTED AGAINST $\mathrm{NSDE1.63}$ BASED ON ALL NUMERICAL RESULTS OBTAINED IN THIS STUDY. A LINEAR FUNCTION COULD BE FITTED OVER THE DATA POINTS (R^2=0.9983) WITH A=0.031 AS THE CONSTANT OF LINEARITY. THE INSET FIGURE SHOWS OUR EXPERIMENTAL DEAN VELOCITIES FROM SINGLE EXPERIMENTS IN TWO DEVICES WITH CROSS SECTIONAL DIMENSIONS OF 100µM×150µM AND 300µM×150µM (CROSS DATA POINTS) THAT FOLLOW THE NUMERICALLY-DETERMINED FIT VERY WELL.

FIGURE 3-1. (A) THE MICROFLUIDIC DEVICE USED FOR SOLUTION EXCHANGE MICROPARTICLES THAT INCLUDED TWO INLETS, TWO OUTLETS, AND AN R=1.185 CM CURVED

MICROCHANNEL (B) MICROPARTICLES DO NOT FOCUS WHEN DEAN DRAG IS THE DOMINANT FORCE. DEAN VORTICES ARE STRONG ENOUGH TO CARRY THE MICROPARTICLES TO THE OUTER OUTLET. (C) INERTIAL FOCUSING OF MICROPARTICLES WHEN THE INERTIAL FORCE IS DOMINANT. INERTIAL FORCE TENDS TO FOCUS THE MICROPARTICLES CLOSE TO THE INNER WALL. HIGHER R_F VALUES CAUSE THE FOCUSING STREAM TO BE NARROWER.

FIGURE 3-2. R_F VS. THE PARTICLE DIAMETER FOR Q= 1 ML.MIN-1 ALONG WITH THE (A) -LOG (DEAN DRAG FORCE) AND (B) -LOG(INERTIAL FORCE). SECONDARY HORIZONTAL AXIS IS NOT DRAWN IN SCALE.

FIGURE 3-3. NUMBER OF MICROPARTICLES DIVIDED BY THE MAXIMUM NUMBER OF MICROPARTICLES IN THE INITIAL SOLUTIONS OF 11 μM AND 4 μM MICROPARTICLES AND THE COLLECTED SAMPLES FROM THE INNER WALL AND OUTER WALL OUTLETS. THE EFFICIENCY WAS 98±0.7%, 86±2% AND 93±0.7% FOR 4 μM, 11 μM AND 19 μM, RESPECTIVELY. THE RECOVERY RATE HAD THE HIGHEST VALUE OF 95 ±1.2% FOR 4 μM. THE RECOVERY RATE DECREASED TO 86±8% FOR 11 μM AND 92±5% FOR 19 μM PARTICLES.

FIGURE 3-4. SEPARATION PURITY REPORTED AS THE PERCENTILE NUMBER OF TARGET MICROPARTICLES DIVIDED BY THE TOTAL NUMBER OF MICROPARTICLES IN EACH OUTLET. SEPARATION PURITY WAS 96±2% AND 89±6% IN THE INNER AND OUTER OUTLETS, RESPECTIVELY.

FIGURE 3-5. QUALITY OF SOLUTION EXCHANGE AND PARTICLE WASHING IN THE MICROFLUIDIC CENTRIFUGE. (A-B) UPSTREAM OF THE DEVICE (CLOSE TO THE INLET) AND THE NORMAL GRAY INTENSITY PLOT ALONG LINE AB (INNER WALL: IW; OUTER WALL: OW). (C-D) THE OUTLET OF THE DEVICE WHERE TB SOLUTION HAS BEEN SWITCHED FROM THE IW TO THE

OW DUE TO CONTROLLED DEAN FLOW AT Q1=Q2=1 ML.MIN^{-1}. THE NORMAL GRAY INTENSITY VALUE SHOWS THAT WATER CONCENTRATION IS HIGH AT A 100 μM DISTANCE FROM THE IW. HOWEVER, FROM 100-200 μM, A MIXED REGION WAS OBSERVED. THE MINIMUM GRAY INTENSITY VALUE WAS MEASURED AT 200-300 μM DEPICTING THE PREVALENT PRESENCE OF TB CLOSE TO THE OW. (G(I)-G(V)) THE INITIAL SOLUTION CONSISTING OF 10% TB AND MICROPARTICLES OF 4 AND 11 μM SIZE (Q1) AND COLLECTED SAMPLES FROM THE OUTLETS (Q3 AND Q4). THE CONCENTRATION OF TB IN THE INNER OUTLET WAS 0.8% (SPECTROPHOTOMETRY TABLE SHOWN).

FIGURE 3-6. CONTINUOUS SEARATION OF BACTERIA FROM PARTICLES USING THE MICROFLUIDIC CENTRIFUGE. (A) INITIAL SUSPENSION CONSISTING OF 19 μM PARTICLES AND E. COLI IN LB BROTH AND COLLECTED SAMPLES FROM THE INNER OUTLET AND OUTER OUTLET. PBS THAT WAS INITIALLY IN THE OUTER TRAVELED TO THE INNER OUTLET AND GOT REPLACED BY LB BROTH. (B-C) PICTURES OF COLLECTED SAMPLES FROM THE INNER AND OUTER OUTLET SHOWING THAT 19 μM PARTICLES WERE FOCUSED CLOSE TO THE INNER WALL AND GOT COLLECTED FROM THE INNER OUTLET WHILE E. COLI REMAINED IN ITS CARRIER SOLUTION AND TRAVELED TO THE OUTER OUTLET. (D) PICTURES OF CULTURED E. COLI THAT WAS COLLECTED FROM THE INNER AND OUTER OUTLETS (E) COLUMN PLOT SHOWING THE PERCENTAGE OF THE CULTURED COLONIES YIELDING A 91±0.5% PRESENCE OF E. COLI IN THE OUTER OUTLET.

Glossary of Terms

Acoustophoresis – Motion of particles in the presence of a sound wave.

Aspect ratio (AR) – Ratio of width of the channel to the height.

Dean Flow – A secondary flow formed in curved channels due to the presence of a radial pressure distribution. This flow results in circulation of fluid particles in the lateral direction of the channel as they move axially forward.

Deionized (DI) water – The commonly used water in laboratories that is free of ions.

Dielectrophoresis – Motion of dielectric particles in the presence of a non-uniform electric field.

Diffusion – The process of moving molecules from a high concentration region to a low concentration region.

Drag force – In fluid dynamics, it is referred to the force that is exerted on an object immersed in a fluid due to the relative movement of the surrounding fluid with respect to the object.

Electrophoresis – Motion of particles in the presence of an electric field

Inertial focusing – Combined effect of shear induced and wall induced lift that causes micron sized particles to focus along specific streams.

ImageJ – A freeware developed by National Institutes of Health that provides a powerful

platform for image analysis.

Laminar flow – A flow regime in which minimum to zero disruption between parallel layers of fluid occurs and is usually characterized by low fluid velocity.

LB – Lysogeny broth (LB) is a nutritious medium that is conventional used for culturing bacteria.

Magnetophoresis – Motion of magnetic particles in the presence of a magnetic field.

Methylene Blue (MB) – With the scientific name of methylthioninium chloride is a blue dye.

Duplex – Processing two particles simultaneously.

Newtonian fluid – A fluid in which the shear stress and shear rate are related linearly

Non-Newtonian fluid – A fluid in which the relation between the shear stress and shear rate is non-linear

Polydimethylsiloxane (PDMS) – An elastomer used for fabricating microfluidic devices by soft lithography.

Photolithography – It is the most widely used process in microfabrication that includes transferring a thin film of a micro-patterned photopolymer onto a substrate by exposing it via a mask to ultraviolet light.

Soft lithography – It is referred to the process of fabricating replicas of a mold using elastomers.

SU-8 photoresist – The most commonly used epoxy in photolithography of microfluidic device molds that can be crosslinked if exposed to ultraviolet light.

Spectrophotometry – A method by which the amount of light absorbed by a substance is measured.

Tween 20 – A detergent that is extensively used for biological purposes such as preparing an oil in water emulsion.

Trypan Blue – It is a blue stain used for selective coloring of dead cell tissues

Chapter 1

Introduction and Thesis Structure

1.1 Background and Motivation

Over the last few decades, microfluidic devices have been successfully used in manipulation of particles in microflow conditions, setting up the stage for integration of laborious steps required in biochemical processes on lab-on-a-chip devices. Recently, there has been an ever increasing demand for integrated microchips that can carry out complex biological tasks consisting of multiple steps rather than performing only a single function[1]. Thus far, many attempts have been made to develop micro-devices for automation of sample handling[2,3], detection and analysis[4,5]. However, in order to fully replicate a complete biological assay, sample preparation needs to be performed on-chip. Nevertheless, due to the inherent complexities in preparing a sample on-chip, there has been a lack of sufficient focus on integration and automation of sample preparation in microfluidics[6].

Sample preparation can be a broad field encompassing cell, particle, or droplet extraction and purification[7,8], concentration[9], dilution[10], sorting[11,12], labeling[13], and washing or solution exchange[14]. A necessary step in sample preparation for biochemical applications is the separation of target particles such as cells from non-target substances and their washing into a clean buffer, which depending on the desired reaction may be required to be done in multiple repeats[15]. Applications of target separation and solution exchange are

not limited to cellular and bacterial manipulation and can be extended to drug delivery and coating of microparticles[16].

The field of microfluidics has shown promising results for providing platforms for performing solution exchange at the microscale. Over the last decade, several techniques have been devised for this purpose that can be classified as active or passive methods. Active methods require an external field for operation while passive approaches do not need any external source of energy.

1.2 Active Microfluidic Devices for Particle Solution Exchange

Various active methods have been proposed since 2004 for automation of particle solution exchange. Active methods, where an external field is essential to transfer the particles/cells from one solution to another, vary from acoustophoretic to magnetophoretic and dielectrophoretic. Generally, in all active methods a straight channel is used through which two streams of fluid, i.e. carrier fluid and clean buffer, are co-introduced. Specific microparticles or cells are isolated and transferred from the carrier fluid into the adjacent target buffer due to their inherent responses to the abovementioned external stimuli.

Hawkes et al.[17] were the pioneers in using acoustophoresis for solution exchange of yeast. In their device, a piezo-ceramic actuator, responsible for producing ultrasound standing waves, was attached to a vertical main duct where cell-free and cell suspension streams were brought into contact. The ultrasound waves exerted an acoustic force on the cells causing them to move to the pressure nodes located in the cell-free solution. Although they could not reach a transfer efficiency of more than 70%, their technique was

a turning point that set the stage for a whole new area of research. A year later, Peterson et al.[18] employed the same concept for solution exchange but with a change made to the geometry. They used a straight channel with a piezo-ceramic plate embedded at the bottom. Two carrier streams along with a clean buffer were co-flown into the channel and the particles were transferred to the clean buffer due to the applied acoustic force (Figure 1-1a). The maximum flow rate was approximately 0.3 mL.min^{-1} while the efficiency was limited to 80%.

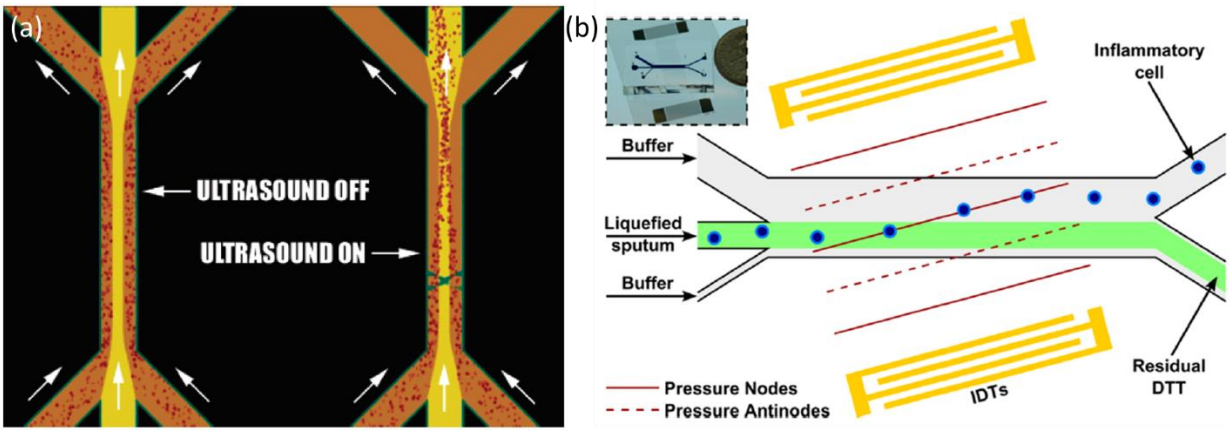

Figure 1-1. (a) Microfluidic device used in the work of Peterson et al.[18] for solution exchange of particles from a solution of Evans Blue. Particles change their solution upon being exposed to the ultrasound-generated acoustic forces in the channel. (b) Solution exchange of inflammatory cells with angled intradigital transducers(IDTs)[19]. Reprinted with permissions from publishers of Ref 18 and Ref 19.

Later on, Augustsson et al.[20] applied a very similar technique for washing and extracting microbeads for de-complexing biofluids. Their device performed the solution exchange in multiple rounds thereby enhancing the purity significantly. However, this was achieved at the expense of limiting the flow rate and recovery rate to 50 μL.min^{-1} and 75%, respectively. Li et al.[21] used intradigital transducers with a tilted angle and achieved recovery rate of 98% and purity of 97% with a flow rate as low as 20 μL.min^{-1}. Recently,

Li et al.[19] showed the application of this method for transferring the inflammatory cells at 1 µL min^{-1} with a recovery rate of almost 84% (Figure 1-1b).

Magneetophoresis is also another active method that has been under focus recently. Peyman et al.[22] introduced a novel microfluidic platform, utilizing magnetic force, for solution exchange of particles. They used a straight channel with four inlets and a magnet placed next to the channel (Figure 1-2a). Co-streams of clean buffer and reagents were flown into the channel. Magnetic particles were introduced through the bottom inlet and got attracted by the magnet through two reagents and two buffer solutions. The particles were then extracted from the top outlet after exposure to the reagents and getting washed by the clean buffer streams. Their device was able to work at a flow rate of approximately 1.8 µL.min^{-1}. Later, in 2009[23], they extended the application of their technique by changing the number of inlet and outlets to carry out multi-step binding of biotin to streptavidin coated magnetic particles. The stock concentration also increased to a maximum amount of 3×10^{8} particles.mL^{-1}. Although their throughput was extremely high compared to previous methods, their devices were not capable of processing more than 25 µL of sample in an hour. The versatility of this technique was further investigated by transferring DNA across multiple streams of buffer and reagents for hybridization and intercalation purposes, and coating magnetic cells by transferring to a polyelectrolyte by Vojtisek et al[24] and Tarn et al.[25], respectively. Tsai et al.[16] used a magnet stack to overcome the interfacial barrier between an aqueous solution and an oil stream to transfer magnetic particles from the former to the latter (Figure 1-2b). This phase change caused a thin layer film of coating (0~1 µm) to morph around the magnetic particle in the course of the transfer. The flow rate inversely affected the thickness of this layer and was varied from

~6 µL.min^{-1} to ~40 µL.min^{-1} corresponding to thicknesses of 1.35 µm to 0.65 µm, respectively. This method proved its competency as a useful tool for transferring synthesized bullet shape particles by Moon et al.[26].

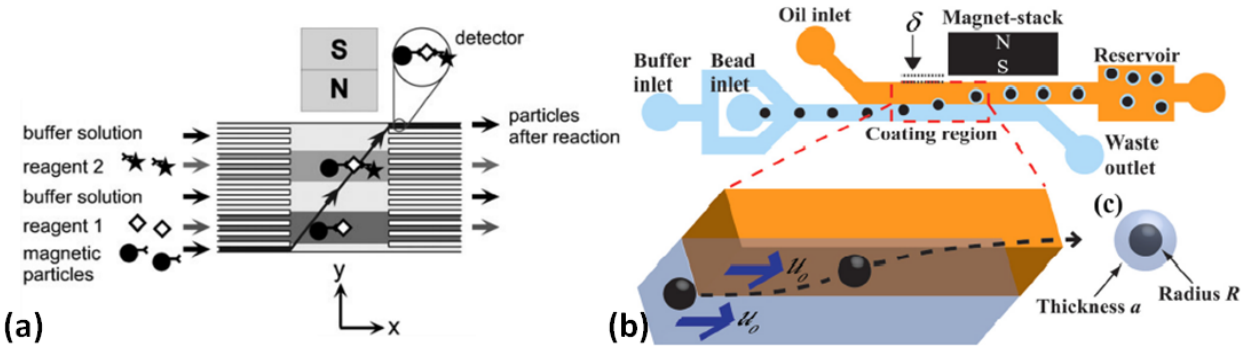

Figure 1-2. (a) Magnetophoretic consecutive washing of magnetic particles in reagent and buffer streams[22]. (b) Magnetophoretic method used by Tsai et al.[16] for solution exchange of magnetic particles from an aqueous solution to oil. Reprinted with permission from publishers of Ref 22 and Ref 16.

Compared to acoustophoretic approaches, magnetophoresis facilitated easier fabrication and higher stock concentration but the achievable flow rates decreased by approximately 10 folds. Also, magnetophoresis is only limited to magnetic particles and cells unless an affinity-based immunomagnetic tagging step is used to magnetize the target non-magnetic particles.

Dielectrophoresis, however, is not developed as much as magnetophoresis and acoustophoresis. In this method, dielectric particles are subjected to a non-uniform electric field[27,28]. The non-uniformity of the electric field causes the particles to experience a net force towards one of the electrodes[29]. This net resultant force is highly dependent on the medium and particle's electrical characteristics and the particle's shape and size[30]. In 2007, Tornay et al.[31] designed a microfluidic channel consisting of three regions, i.e. pre-focusing region, exchange region and extraction region (Figure 1-3a). In the pre-

focusing region, microparticles were focused close to the channel wall due to the inertial force (discussed later). Upon pre-focusing, the particle suspension and the clean buffer were brought into contact. As a result of pre-focusing, the particles laid very close to the interface thereby only a small force was needed to push them to the clean buffer. This force was secured by the dielectrophoresis force in the exchange region. In the extraction zone, the fluid streams got separated, exiting from different outlets for extraction. Their device had a flow rate limit after which the efficiency dropped dramatically. For 0.5-2 µm particle sizes, the maximum flow rate was approximately 0.024 $\mu L.min^{-1}$ to 0.24 $\mu L.min^{-1}$. They assumed that the fluorescent intensity of particles at the outlet reflects the particles density and claimed an efficiency of close to 100% within their flow rate limit. Park et al.[32] used two pairs of interdigitated electrodes at 45° and 90° angles for solution exchange and concentration of bacterial cells (Figure 1-3b). The first set of electrodes were used to move the bacterial cells from a sample stream to a buffer stream and the second set was employed for increasing the concentration of bacteria by up to 10^4 folds. They could achieve the efficiencies of 97%, 94.3% and 87.2% at 0.5 $\mu L.min^{-1}$ for beads in TAE buffer, *E. coli* in human cerebrospinal fluid and *E. coli* in blood, respectively. Dielectrophoretic devices are relatively difficult to fabricate compared to the other techniques and work at lower flow rates, thus their application is limited for sample preparation.

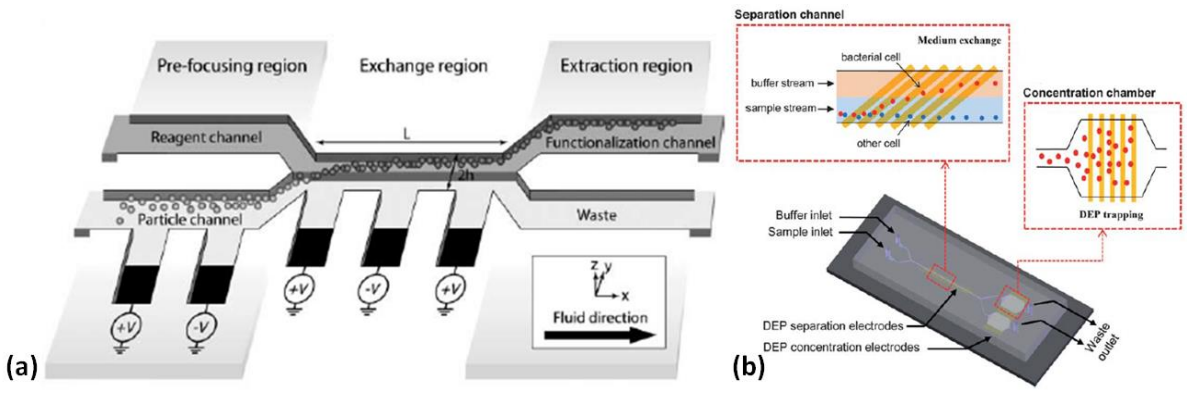

Figure 1-3. (a) Dielectrophoretic solution exchange technique developed by Tornay et al.[31] *(b) Angled electrodes used by Park et al.*[32] *for dielectrophoretic solution exchange. Reprinted with permission from publishers of Ref 31 and Ref 32.*

1.3 Passive Microfluidic Devices for Particle Solution Exchange

Current passive methods for solution exchange and cell washing mostly rely on manipulating the location of microparticles using inertial and drag forces in straight and curved channels. Inertial force consists of two components, i.e. wall-induced and shear gradient lift forces[33]. As a particle approaches the wall of a confined channel with a comparable size, the streamlines surrounding the particle tend to divert to the side that is away from the wall thus resulting in a pressure build up at the wall side (Figure 1-4a). This results in a wall-induced lift force (F_w) away from the wall (towards the center) that decreases as the distance from the wall increases[33].

$$F_w = \rho U_{max}^2 C_w a^6 / D^4 \quad (1)$$

where ρ shows the fluid density, U_{max} is the maximum fluid velocity, C_w is a constant that depends on the distance from the wall, and a and D are particle diameter and hydraulic diameter of the channel, respectively.

Shear gradient lift stems from the parabolic nature of the velocity profile in straight channels. Curvature in the velocity profile causes the fluid velocity to be different on either side of the particle (Figure 1-4b), if a/D_h ratio is greater than 0.07[34]. The particle has a tendency to reduce this velocity difference, hence migrating to channel regions where velocity difference is minimized, i.e. away from the center. Therefore, the shear gradient causes a net force toward the walls of the channel (Figure 1-4b). Shear gradient force (F_L) can be estimated using the following formula[33].

$$F_{SG} = \rho U_{max}^2 C_w a^3 / D \tag{2}$$

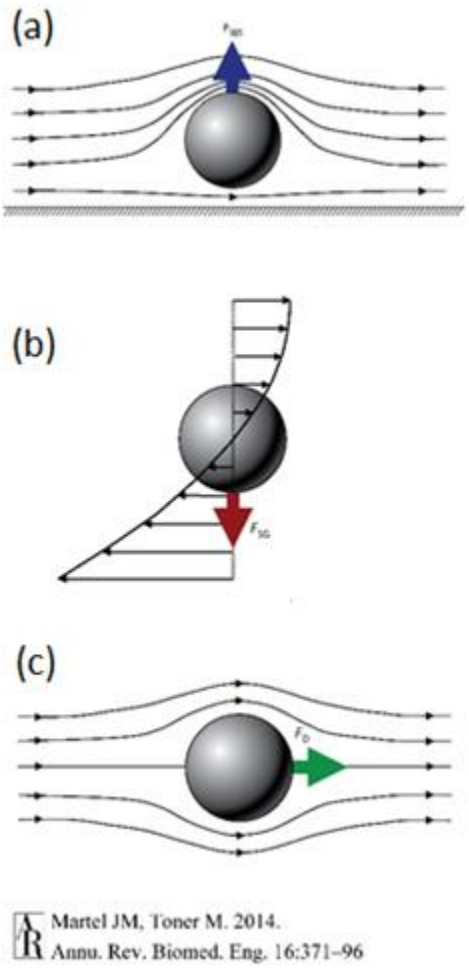

Figure 1-4. (a) Flow streamlines around a particle approaching the wall. (b) Relative velocity of a particle in poiseuille flow. (c) Stokes Drag acting on a particle in curved channel. Reprinted with permission from publishers of Ref 33.

Particles moving across streamlines with a set velocity experience drag force that follows Stokes drag force formula (Figure 1-4c). Stokes drag changes linearly with the particle diameter and is expressed by the following formula:

$$F_L = 3\pi\mu a U_{SF} \quad (3)$$

where μ represents the fluid dynamic viscosity and U_{SF} is the particle's lateral velocity. This formula is limited to Reynolds number (Re) of lower than 1 where Re= $\rho U_{SF} D/\mu$.

Gosset et al.[35] took advantage of the above-mentioned forces and fabricated a straight channel with two inlets through which the microparticles exchanged their solution by the virtue of the inertial force (Figure 1-5). In their technique, that is called rapid inertial solution exchange (RInSe), the stream of the carrier fluid was introduced from the top inlet and was brought into contact with the clean buffer running through the bottom channel. The particles experienced a net inertial force toward the clean buffer that occupied more space in the width of the channel. Therefore, the particles got transferred to the clean buffer and were extracted with an efficiency of close to 90%. Dudani et al.[15] employed RInSe[35] for a biological application and successfully expanded its application to microvesicles. Although the inertial focusing helped removing the necessity of using the external field for solution exchange, it was limited to flow rates of approximately 70 µl.min^{-1} and throughput of 1000 particle.s^{-1}.

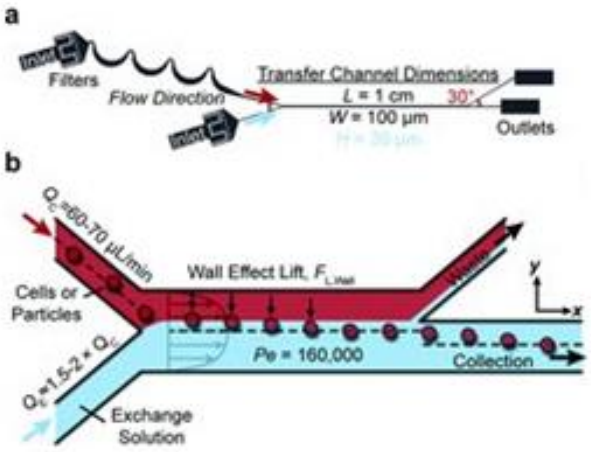

Figure 1-5. Passive method for exchanging the solution of particles. (a) Schematic of the setup of the RInSe method consisting of two inlets and a straight microchannel with a length and width of 1cm and 100 µm, respectively. (b) Inertial force pushes the particles to move to the clean buffer[35]*. Reprinted with permission from publishers of Ref 35.*

In another effort, Sollier et al.[36] used a combination of micro-vortices and inertial lift force to trap large particles and sequentially release and wash them with a buffer solution. Their device consisted of 8 straight channels followed by downstream expansion-contraction trapping regions (Figure 1-6). Particles that were distributed randomly in the inlet got inertially focused on their equilibrium streamlines in the straight channels. In the trapping region, however, the shear gradient lift causes the larger particles to get trapped in the rectangular expansion reservoirs. They next run another particle-free clean buffer through the channel to wash and collect the trapped particles. The purity of this method was 80-100% while the efficiency varied extensively based on the type of the cells that were used. However, their efficiency is considered low compared to other passive techniques. Also, this method is limited to larger particles and has the disadvantage of being discontinuous.

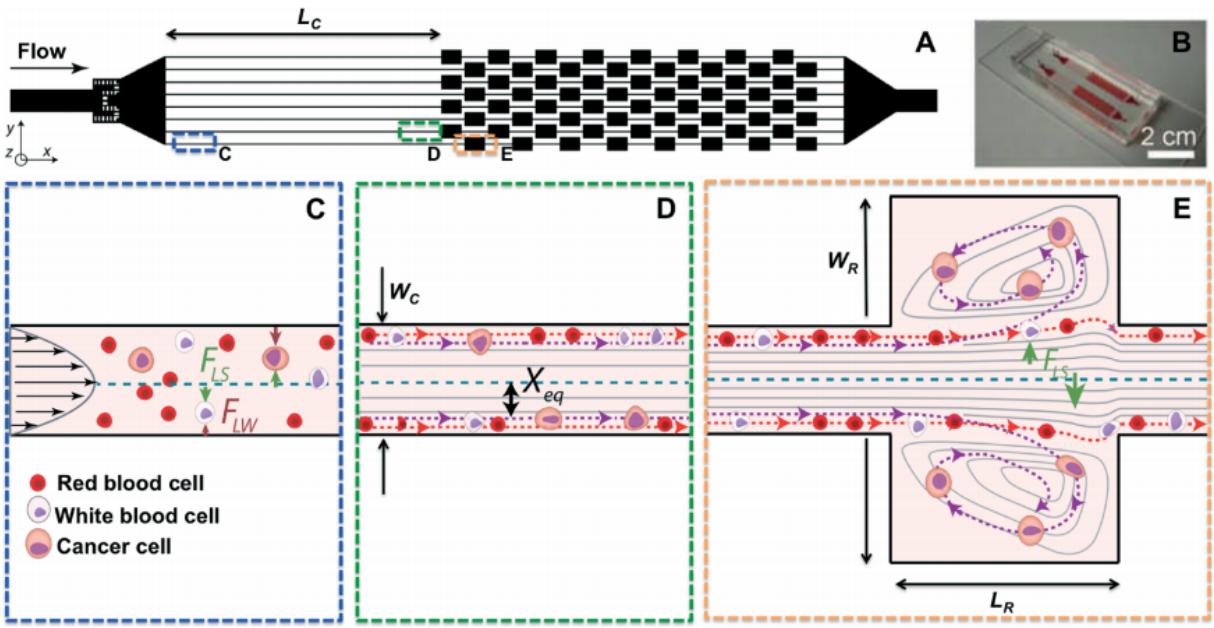

Figure 1-6. (A-B) Schematic and the device used by Sollier et al.[36] for discontinuous particle washing. (C) Particles were randomly distributed in the inlet and (D) got focused due to the inertial force. (E) Shear gradient lift caused the particles to get trapped in the rectangular expansion regions. Particles got subsequently washed by running another buffer trough the device. Reprinted with permission from publisher of Ref 36.

As another example, Ha et al.[37] could transfer microparticles from a non-Newtonian fluid to a Newtonian fluid in a straight microchannel by carefully controlling the viscoelastic and inertial forces. This was not feasible before since the flow condition required to manipulate particles in a commonly used non-Newtonian fluid (polymeric solution of poly(ethylene oxide)) is order of magnitudes different from the one for a Newtonian fluid. This was overcome by increasing the relaxation time of the non-Newtonian fluid via using λ-DNA. They could transfer microparticles with high purity (>97%) and over a broad flow rate spanning 2 orders of magnitude (0.4-40 µl.min^{-1}). Although this was a great technical achievement, the working flow rate in this system was still limited to a maximum of 40 µL.min^{-1}. Lately, Deng et al.[38] extended the application of microfluidic based solution exchange to droplets (Figure 1-7). They reported successful accomplishment of solution

exchange of water droplets across oil-oil interfaces and oil droplets across water-oil interface in their experiments at a maximum rate of approximately 20 droplet.s^{-1}. Solution exchange of the droplets was based on the difference between interfacial forces of the fluids. Droplets changed their solution to reduce the interfacial energy of the system. Therefore, they encountered a limitation in terms of selecting the proper fluids and could not achieve solution exchange for flow rates higher than 1 mL.hr^{-1}.

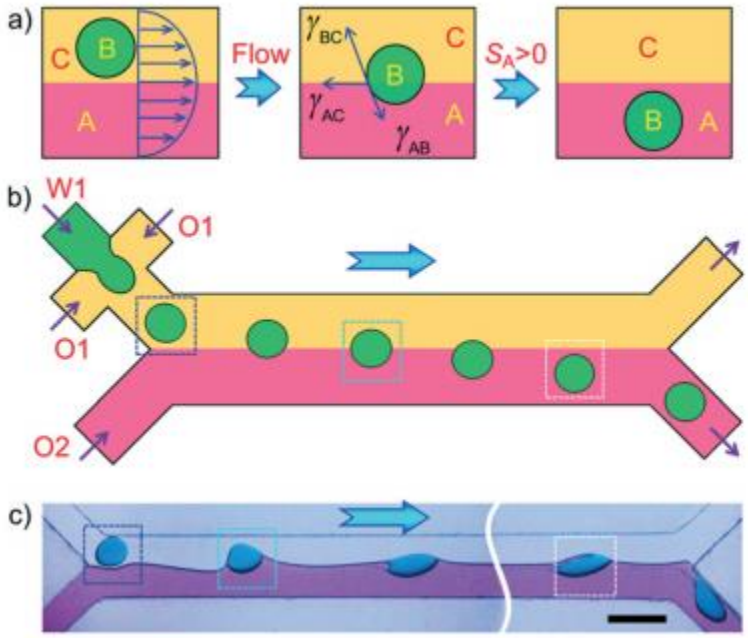

Figure 1-7. (a) Interfacial forces that droplets encounter at the interface of the fluids in the work of Deng et al.[38] *(b-c) Schematic and actual images of the device. Reprinted with permission from publishers of Ref 38.*

1.3 Knowledge and Technological Gaps

Active methods can enhance the specificity and normally work at slightly higher flow rates compared to the passive methods but they are expensive to run and are cumbersome to fabricate requiring multiple fabrication steps. Therefore, recently the focus has shifted

towards devising and developing passive devices for solution exchange of cells and microparticles.

Although passive methods are advantageous in terms of being independent of any external field, they are still limited to low flow rates and cannot be practical where high flow rate and throughputs are required. For example, according to the guideline "ISO707:2008, Milk and milk products: Guidance on sampling", an aliquot of milk should be at least 25g (~25 ml) to be considered a valid representative of the original sample[39]. Consequently, a microfluidic device designed to analyze milk should be capable of processing such volumes in a reasonable amount of time (e.g. 15-30min).

Based on the above-mentioned limitations and requirements, there is a need for a solution exchange microdevice with the following characteristics.

1- Operable at high flow rates of ~1 $mL.min^{-1}$ and higher.
2- Capable of performing solution exchange at throughputs of more than 10^4 $particle.s^{-1}$.
3- High purity solution exchange performance to avoid contaminating the clean buffer (>95%).
4- High efficiency in washing and isolating target particles from non-targets (>90%).
5- Simplicity in design and fabrication so it can be used at point-of-care.
6- Independency of any external field in order to be usable in remote areas or for point-of-care applications.
7- Independency of using sheath flow (unless as a target fluid) since it dilutes and contaminates the sample.

1.4 Goal and Objectives of the Thesis

In previous studies, focus has been placed solely on particle manipulation and its motion from one liquid to another as a means to exchange solutions. This led to low flow rate and throughput (below 100 $\mu L.min^{-1}$) in passive systems and higher cost of the external field in active methods. However, in this thesis, we hypothesized if accurate manipulation and control of both fluids and particles can be used simultaneously to enhance the throughput of particle solution exchange in high-volume fluidic samples. Therefore, we aimed to devise a novel passive method for rapid exchange of particles' solution in a curved microchannel that is applicable for high volume processing and is highly efficient, reliable and applicable for a wide range of particle sizes. We utilized the secondary flow based recirculation behavior of co-laminar flows in curved microchannels for controlling the fluid around particles and inertial-Dean coupled particle focusing for manipulating the particles. To achieve our goal, the following objectives were pursued.

1- Study of fluid manipulation by investigating the Dean flow based fluid recirculation behavior in curved microchannels.
2- Study of particle manipulation by investigating the inertial-Dean coupled focusing of particles in curved microchannels.
3- Design of a curved microchannel solution exchanger to achieve both particle focusing and fluid switching at the same time.

1.5 Chapters Organization

In chapter 2, we have addressed the objective 1 of the thesis. Here, we used co-flows of

coloured liquids in curved microchannels with different radii of curvatures, and monitored the Dean flow based lateral displacement of fluids using optical microscopy. A quantitative *Switching Index* parameter was introduced to calculate the average recirculation Dean velocity in these channels. Additionally, we developed and validated a numerical model to expand our investigations to elucidating the effects of channel hydraulic diameter, width, and height as well as fluid kinematic viscosity on Dean velocity. Accordingly, a non-dimensional comprehensive correlation was developed based on our numerical model and validated against the experimental results. The proposed correlation can be used extensively for the design of curved microchannels for manipulation of fluids, particles, and biological substances in spiral microfluidic devices.

In chapter 3, our focus shifts to studying the inertia-based focusing of particles in curved microchannels to achieve objectives 2 and 3 of this thesis. In this chapter, we will introduce the main forces involved in determination of the position of microparticles in a curved microchannel. Two regimes of focusing, i.e. inertia- and drag-based, will be defined and the range of particle sizes for each regime will be determined quantitatively. Last two sections of this chapter will be dedicated to objective 3 where we combine the knowledge of fluid switching and particle focusing to design a microfluidic device for solution exchange of particles. The suitability of this technique for high throughput solution exchange of biological samples will be demonstrated at the end of chapter 3.

In chapter 4, the major outcomes of the thesis and the opportunities for future research will be discussed.

Chapter 2

Semi-Empirical Estimation of Dean Flow Velocity in Curved Microchannels[1]

2.1 Introduction

Curved and spiral microchannels have a wide range of applications in microfluidic devices[40,41] such as isolation of circulating tumor cells[42], cell enrichment[43], bacteria separation[44], fluid mixing[45,46], microfilteration[47], and inertial focusing and separation of particles[34,48–52]. Fluids flowing in the axial direction of a curved channel experience a pressure gradient along the radial direction[52]. This leads to continuous circulation of the fluid in the radial direction and subsequent formation of two or more counter-rotating vortices in the channel[53-54]. This lateral recirculating flow is called a secondary (or Dean) flow[55–57](Figure 2-1). Formation of Dean flow in curved and spiral channels is inevitable, yet their presence may be dominant and useful in some applications[58–60] while undesirable in others[61,62].

Understanding the causes and effects of Dean flow in curved channels is of paramount importance to the design of microfluidic devices. For instance, it has been reported that secondary flows can skew the velocity profile in arterial bends and affect the shear

[1] A version of this chapter is submitted to Nature Scientific Journal. P. Bayat and P. Rezai, Sci. Reports (Nature Publ. Group), 2017, submitted.

distribution in blood vessels[63]. This influences low-density lipoproteins (LDL) transport through the vascular network and enhances the risk of atherosclerosis[64,65]. As an additional example, Martel and Toner[66] reported the necessity of the existence of an accurate formula to predict the velocity at which particle focusing occurs in a spiral channel. They took two different theoretical approaches to investigate the inertial focusing, one by ignoring and the other by including the Dean velocity (V_{De}). Using the former approach, they could only determine the width required for particle focusing. However, by numerical simulation of Dean flow in their channel, they could calculate the average V_{De} required for the later approach to find both the width and axial velocity required for inertial focusing. Accordingly, predicting the Dean flow characteristics in curved microchannels, and specifically the average Dean flow velocity, with respect to fluid properties (e.g., density and viscosity) and channel specifications (e.g., width, height and radius of curvature) has been the center of attention of a few research articles[34,67].

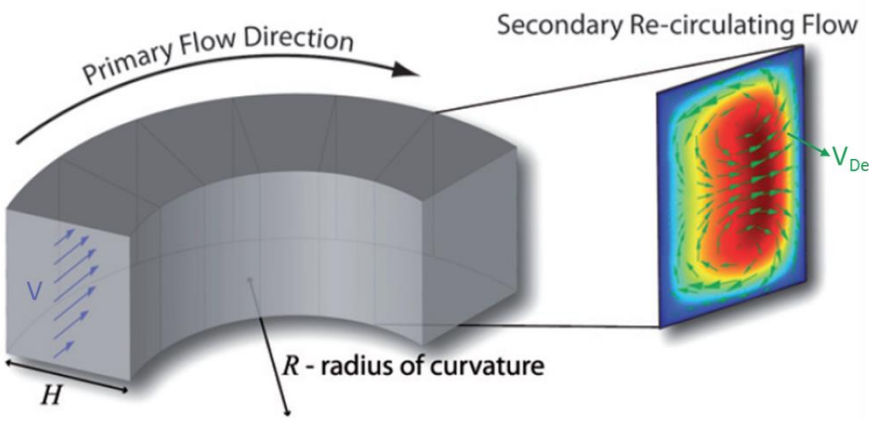

Figure 2-1. Formation of two counter rotating vortices (i.e. secondary Dean flow) in a curved microchannel. Reprinted with permission from publisher of Ref 80.

Attempts to characterize the Dean flow in curved microchannels can be categorized to the use of analytical, numerical and experimental approaches. Two dimensionless numbers, namely the Reynolds (Equation 4) and the Dean (Equation 5) numbers, are

used widely to describe the primary and secondary fluid flow behaviors in a channel.

$$Re = \frac{\rho V_x D}{\mu} \tag{4}$$

$$De = Re\sqrt{\frac{D}{2R}} \tag{5}$$

where ρ [kg.m^{-3}] and μ [Pa.s] denote the fluid density and dynamic viscosity, respectively. Geometrical properties of the channel are represented by *D* [m] and *R* [m] which are the hydraulic diameter and radius of curvature of the channel. Lastly, V_x [m.s^{-1}] is a characteristic velocity that is often taken to be the average axial velocity of the fluid. Reynolds number presents the ratio of inertial forces to viscous forces and is a representative of the fluid flow regime. Fluid flow in curved channels is highly influenced by the lateral acceleration of the fluid due to centripetal forces. Dean number indicates the ratio of the inertial and centripetal forces to the viscous forces[68] and is widely used to characterize the strength of secondary flows in curved channels[69]. Dean number commonly alters in the range of 0-30 in microfluidic devices[49,57].

The exact analytical solution of Navier-Stokes equations for fluid flow in curved microchannels does not still exist but efforts have been made to simplify these highly nonlinear coupled equations and solve them using mathematical approaches such as perturbation and spectral methods. Norouzi and Biglari[70] used curvature ratio as the perturbation parameter to solve the secondary flow problem in curved ducts. Although their solution showed acceptable agreement with experimental results but associated errors were remarkably high for sharp curvatures that are prevalent in microfluidic devices. Dual solutions for circular curved tubes were proposed by Yanase et.al[71] but the high Dean number in their solution (order of 1000) is not directly applicable to microfluidic applications in which the Dean number is relatively low (De<30). Analytical solutions for

elliptical[72] cross sections and non-Newtonian fluids such as Bingham Plastics[73] and second order fluids[74] have also been reported using the perturbation method. However, extensive simplifications in analytical solutions limit their application for real life problems and make them not suitable for investigation of secondary flows in curved microchannels especially if multi-phase flows (e.g., particles in water) are to be investigated. Therefore, analytical methods have not been successful yet to offer a reliable solution that can conveniently be used for determination of Dean flow velocity at low Dean numbers in microfluidic devices.

Zhang et al.[75] took a numerical approach to investigate the effects of Coriolis and centrifugal forces on flow patterns (De>100) and the friction factor in square and rectangular channels with aspect ratios of lower and higher than one. Their observations led to the conclusion that four types of vortices can co-exist in the channels due to the effects of centrifugal and Coriolis forces and their associated instabilities. Ookawara et.al[67] numerically studied Dean flows in a rectangular curved microchannel and proposed two correlations, both in the form of power functions, for estimation of average (Equation 6) and maximum Dean flow velocities.

$$V_{De} = 1.8 \times 10^{-4}\, De^{1.63} \quad \frac{m}{s} \tag{6}$$

Although the correlations proposed by Ookawara et al.[67] have been widely adopted for design of spiral microchannels, the effects of many influential parameters such as fluid viscosity and channel hydraulic diameter, aspect ratio, and radius of curvature were not investigated in-depth. Altogether, there is a need for development and experimental validation of numerical models that can provide a more accurate estimation of the average Dean flow velocity in spiral and curved microchannels.

At the experimental level, Ligrani and Niver[76] studied the effect of Dean number (40<De<220) in a curved channel with large aspect ratio (width/height) of 40 and reported formation of counter-rotating vortices for Dean numbers greater than 64. A set of experiments in a square curved channel were performed by Bara et. al,[77] and their results revealed formation of two or four symmetric vortices at De=125 and De=137, respectively, demonstrating the importance of channel dimensions and fluid properties in formation of secondary flows. Yamamoto et al.[78] experimentally visualized secondary flow vortices in a curved channel with rotating and stationary walls. They characterized the shape of Dean flow vortices for different Taylor (Tr=$\frac{w^2\Omega}{\sqrt{2\delta\nu}}$, where w is the width of the channel, and Ω, δ and ν are angular velocity, non-dimensional curvature and kinematic viscosity, respectively) and Dean numbers in a square cross section channel and provided a flow pattern diagram showing the layout and number of vortices on various Tr-De diagrams. Dispersed microparticles can also be used for flow visualization and velocity field determination[79], however, it has been already demonstrated that particles are greatly affected by inertial forces[80] in straight and spiral microfluidic devices and specially when the size of the channel is comparable to the size of the microparticles. Thus, particles recirculation velocity may not be the best representative of Dean flow velocity in a curved microchannel. There is a need for development of more reliable experimental approaches for parametric investigation of the average Dean velocity in spiral and curved microfluidic devices.

In this chapter, we have investigated the effect of various deterministic parameters on Dean flow velocity in curved microchannels using simple but practical experimental and numerical approaches. The studied parameters can be categorized into geometrical

characteristics (e.g. channel width, height, hydraulic diameter, and radius of curvature) and fluidic properties (e.g. axial velocity and kinematic viscosity). With this comprehensive investigation, we were able to propose a non-dimensionalized correlation for estimation of V_{De} in curved microchannels (at De<30) that can be used widely for design of curved and spiral microfluidic devices.

2.2 Materials and Methods

2.2.1 Device Design

The microfluidic devices used in this study were made of polydimethylsiloxane (PDMS) and consisted of a curved microchannel with θ=330^0, two inlets and two outlets as shown in Figure 2-2a. The effect of radius of curvature (R=0.5, 1, 1.5 and 2 cm) on fluid recirculation (schematically shown in Figure 2-2b) and Dean flow velocity (V_{De}) was investigated in square cross-section (150µm×150µm) curved microchannels. Two additional devices with R=1 cm and rectangular cross-sections of 100µm×150µm and 300µm×150µm were used to investigate the effect of channel dimensions (width, height and hydraulic diameter) on Dean flow velocity. Two additional properties studied were fluid axial velocity (V_x) and kinematic viscosity as fully discussed in the following sections.

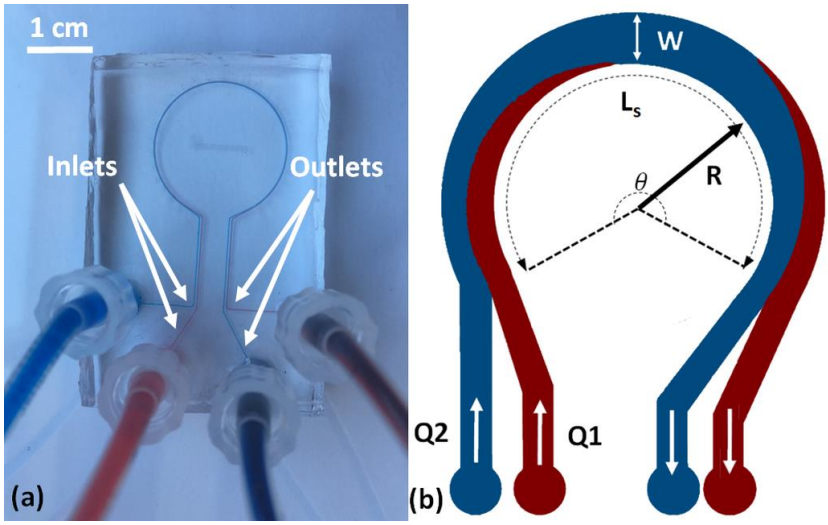

Figure 2-2. A microfluidic device consisting of a curved microchannel with a radius of curvature of R=1 cm and cross section area of w=300μm by h=150μm that was used for experimental investigation of average Dean velocity (V_{De}). (a) Water streams dyed with methylene blue and red food dye were introduced from the two inlets and their radial displacement was imaged. This is demonstrated schematically in (b). Microchannels with four radii of curvatures (R=0.5, 1, 1.5 and 2 cm all with 150μm×150μm cross-section) and two additional cross-sectional dimensions (100μm×150μm and 300μm×150μm both with R=1 cm) were used in our studies.

2.2.2 Device Fabrication

Standard photolithography[81] and soft lithography[82] methods were used to fabricate the abovementioned microfluidic devices. In order to prepare the master replication molds, negative SU8 2075 photoresist (Microchem Corp., MA, USA) was spun over 4-in diameter silicon wafers which were obtained from University Wafers Corp. (MA, USA). Coated wafers were then prebaked at 65^{0}C for 5 minutes and 95^{0}C for 30 minutes followed by exposure to ultraviolet light through a photomask. Post-bake treatment was carried out at 65^{0}C and 95^{0}C for 5 and 12 minutes, respectively. The process was finalized by dissolving the unexposed SU8 using SU8 developer solution. Subsequently, degassed mixture of 10:1 ratio PDMS pre-polymer base and curing agent (Sylgard 184 kit, Dow Corning, MI, USA) was poured over the mold and heated at 80℃ for 2hr. The cured PDMS layer was peeled off the master mold and holes were punched on it at inlets and outlets of the microchannel. In order to enclose the microchannel, an oxygen plasma

machine (Harrick Plasma, PDC-001, NY, USA) was used to bond cured PDMS layers with glass slides at 45W for 30-35s, followed by heating at 80℃ for 5-10 minutes to enhance the bonding. To prepare the device for experiments, Tygon tubes (Saint-Gobain, Paris, France) were connected to the punched inlets and outlets of the bonded device.

2.2.3 Experimental Setup and Procedures

Two 10 mL syringes containing Methylene Blue (MB) dyed and tap water were installed onto a dual syringe pump (Legato 110, KD Scientific, USA) and used to co-flow the fluids with favorable flow rates into the microfluidic device that was positioned under a microscope for optical imaging. In order to investigate the effect of viscosity on Dean velocity, we used water and glycerol mixture with 15% volumetric ratio while viscosity and density values of the mixture were calculated from the work of Cheng[83]. Inlet flow rate was changed from 0.2-1 $mL.min^{-1}$ (corresponding to axial velocity of V_x=0.15-0.74 $m.s^{-1}$ and Re= 22.5-112.5) and flow was allowed to stabilize in the devices for 2 min. After flow stabilization, a video from the entire channel, from inlet to outlet, was recorded at a 5x magnification via a camera (Point Grey, BC, Canada) connected to the inverted microscope (Bioimager, ON, Canada). Devices were properly washed after each experiment with water for at least 5 minutes to remove any MB residue. Experiments were repeated at least three times for each flow rate and viscosity setting to obtain average and standard deviation values at each experimental condition.

2.2.4 Numerical Model

We used COMSOL Multiphysics to simulate the above-mentioned curved microchannels used in our experiments. All of the simulations were performed using the laminar flow module. The 3D geometry of the model consisted of a 60^0 portion of a curved

microchannel with a specific width and height (Figure 2-3a). Dynamic viscosity and density of water were set to 0.001 Pa.s and 1000 $kg.m^{-3}$, respectively. The corresponding properties of water-glycerol mixtures were extracted from the work of Cheng[83] and set manually in our model. The inlet, outlet and wall boundary conditions were set as flow rate (0.2-1 $ml.min^{-1}$), atmospheric pressure and no slip boundary conditions, respectively. We used COMSOL Multiphysics' mesh module to mesh the geometry. Square and triangular mesh elements with various number of mesh elements were tested and triangular elements were selected (Figure 2-3b). The number of mesh elements varied from 10^5 to 10^6 depending on the hydraulic diameter of the channel. Also, the number of the elements increased closer to the channel wall to be able to compensate for the severe gradients in the boundary layer region. We used a linear solver with iterative method (GMRES) left preconditioning with maximum iteration number of 200 to solve the Navier-Stokes equation for velocity and pressure as dependent variables (Figure 2-3(c-d)). Upon solving the equations, a cross section of the channel located at 10^0 before the outlet was analyzed and the average lateral velocities over this cross section were calculated and reported as the average Dean velocities (V_{De}). The average V_{De} was calculated by deriving the average tangential velocities over the cross section of the channel normal to the wall. We decreased the size of the modeled channel to a shorter length to enhance our computation speed and accuracy. The average V_{De} along the channel was calculated and no significant changes in V_{De} was observed after 60^o, so we modeled only a 60^o portion of the channel. In order to prevent the outlet boundary condition from affecting the results, we calculated the average V_{De} at a cross-section that was located 10^o before the outlet.

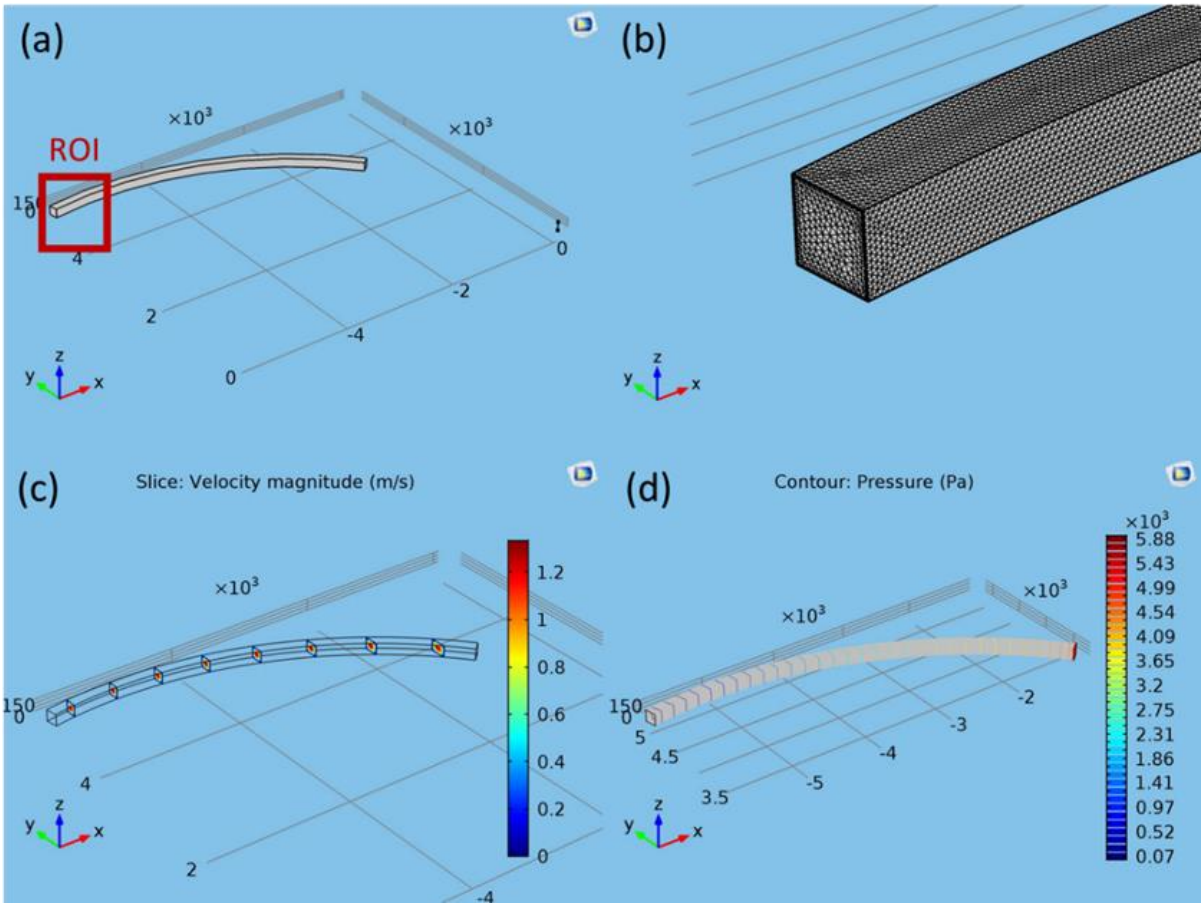

Figure 2-3. Numerical model used for determination of Dean velocity. (a) Geometry of a microchannel with R=0.5 cm and cross-sectional dimension of 150μm×150μm. (b) Mesh elements in the Region Of Interest (ROI) shown in (a). The number of mesh elements increased at the wall. Total number of elements were approximately 8×10^5. (c) Velocity distribution over yz-planes for water at De=12. (d) Pressure contours for the geometry presented in (a) and the flow conditions mentioned in (c).

2.3 Results and Discussion

2.3.1 Quantification of Dean Flow in Curved-Channel Microfluidic Devices using a Switching Index (SI)

We first focused on developing a simple and accurate experimental technique to quantify average Dean velocity in our curved-channel microfluidic devices. For this, methylene blue (MB) and water solutions were co-flown into the devices at different axial velocities and videos of fluid recirculation were recorded along the channel under a microscope. The videos were then imported into the freeware ImageJ (National Institutes

of Health, Bethesda, Maryland, USA) for analysis of target cross sections along the curved microchannels. For instance, Figure 2-4a shows the snapshots of the R= 1cm device along the channel with a co-flow of water and MB at a flow rate of 0.6 mL.min^{-1} (V_x=0.22 m.s^{-1}).

Intensity values (c_i) across assessment lines (e.g. line AB in Figure 2-4a) drawn at 10 degree intervals along the channel were obtained (Figure 2-4b) and an average intensity ($\bar{c}$) for each analyzed line was calculated from the obtained cross-sectional intensity values. To obtain a quantitative assessment of the secondary Dean flow and fluid recirculation, the intensity values obtained in Figure 2-4b were used in Equation 7 to calculate the σ-values (standard deviation of intensity values) at each assessment line AB along the channel. Subsequently, a normalized index called the *Switching Index* (SI) was derived for each assessment line using Equation 8 and plotted along the channel for quantification of Dean flow characteristics such as Dean velocity. The *SI* was defined based on an index originally used to characterize mixing in microfluidic devices.[84] However, diffusive mixing was not significant in our device (Peclet number ~ 10^5) due to the high axial flow velocities while the *SI* trends properly represented the lateral displacement of fluids due to Dean flow in our curved microchannels.

$$\sigma = \sqrt{\frac{1}{N}\sum_{i=1}^{N}(c_i - \bar{c})^2} \tag{7}$$

$$SI = \sigma/\sigma_{max} \tag{8}$$

In Equation 7, N denotes the number of points analyzed along the assessment line AB at each cross section.

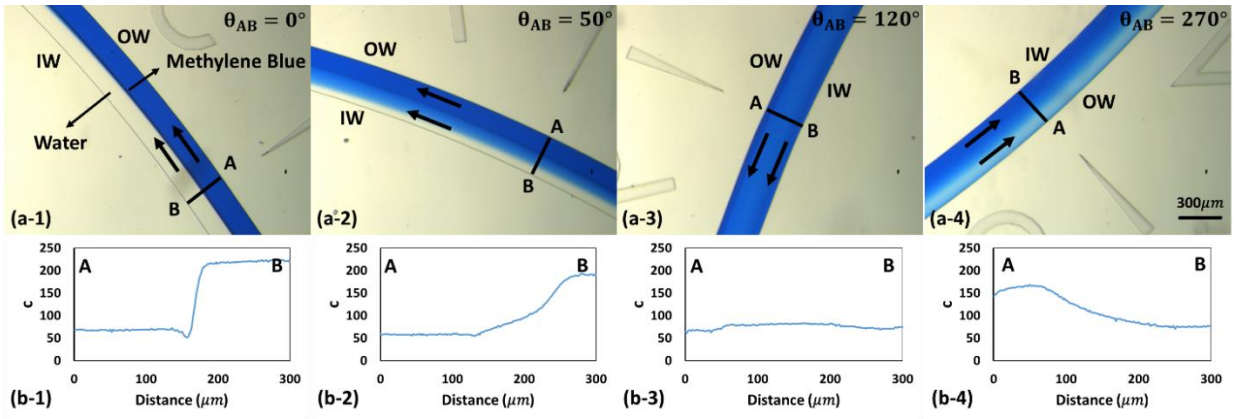

Figure 2-4. Co-flow images of methylene blue (MB) and water at inlet flow rate of 0.6 mL.min^{-1} (i.e., velocity of 0.22 m.s^{-1}) along the length of a 300μm×150μm curved microchannel with R=1cm (a-1 to a-4) and intensity diagrams corresponding to assessment lines AB along the width of the channel at specific control points in each image (b-1 to b-4). (a-1 and b-1) show the beginning of the channel where the intensity diagram was similar to a step function and the fluids were completely separated, i.e., water at Inner Wall (IW) and MB at Outer Wall (OW). In (a-2 and b-2), MB and water started to displace laterally due to Dean flow vortices. In (a-3 and b-3), water was completely sandwiched in between MB layers, and the intensity diagram was almost uniform. In (a-4 and b-4), water and MB started to appear closer to the OW and IW, respectively, hence demonstrating switching in position compared to their initial conditions.

2.3.2 Estimation of Switching Length and Time using the SI

We first investigated the suitability of the SI in Equation 8 for investigating the Dean flow-based recirculation of fluids and quantifying the switching length (L_s) and time (t) at which water and methylene blue solutions exchange radial positions in a curved microchannel. For this, we conducted a series of experiments with the microfluidic device that had a radius of curvature of R=2 cm and cross-sectional dimensions of 150μm×150μm. Methylene blue and water solutions were co-injected into the device at various axial velocities (V_x=0.15-0.74 m.s^{-1}) and the effect of fluid axial velocity on SI was investigated along the channel length. The results are shown in Figure 2-5.

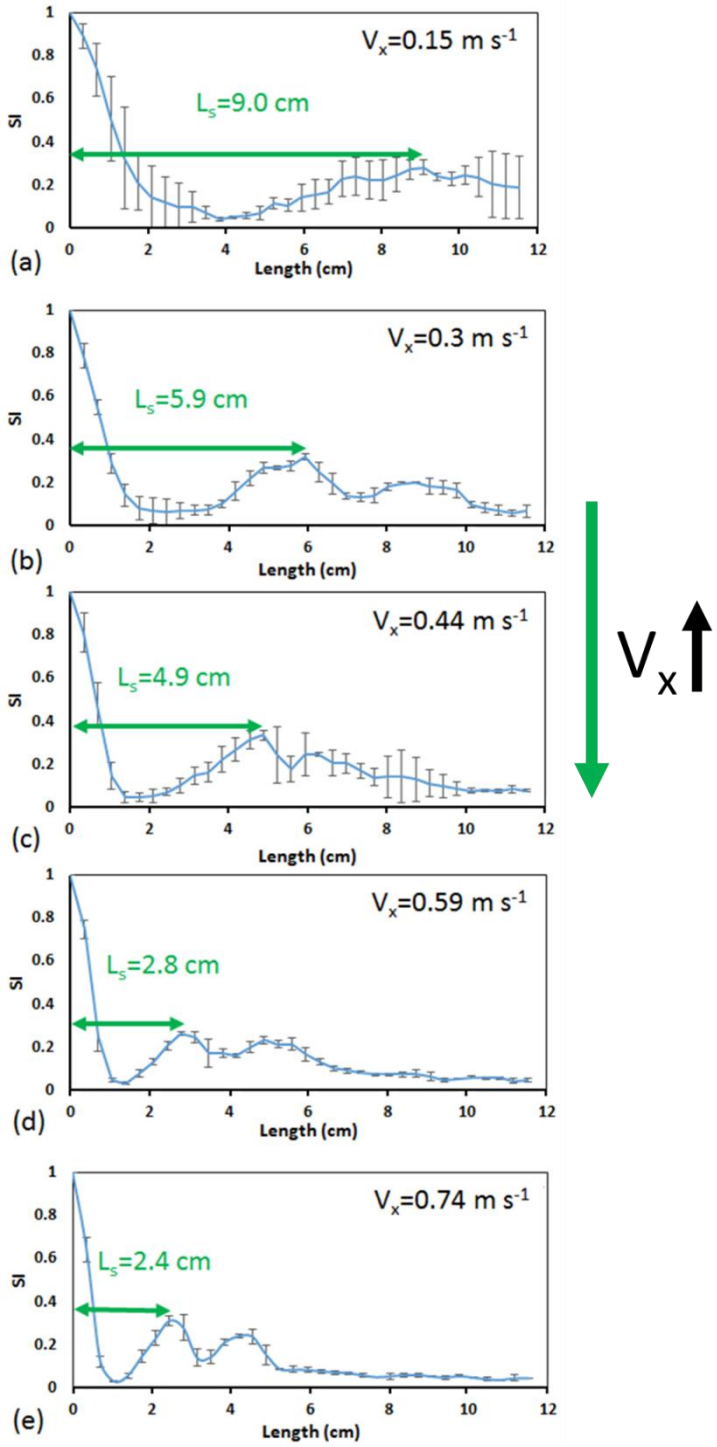

Figure 2-5. Switching Index (SI) diagrams along the length of the channel at various inlet axial velocities, V_x, of methylene blue and water that were co-injected into a device with R=2 cm and cross section area of 150µm×150µm. SI decreases along the channel as the two solutions form counter-rotating vortices and increases when they start separating from each other into distinct phases again downstream the channel. The first peak in the SI plot indicates the exact location of the first switch in position (L_s) of methylene blue and water solutions (i.e., 180º recirculation). At higher axial velocities, a second switch corresponding to a full 360º recirculation of fluids can be clearly seen. Error bars represent the standard deviation of three experimental repeats.

As shown in Figure 2-5, the SI was equal to unity at the entrance of the channel ($\sigma = \sigma_{max}$ in Equation 8) where the methylene blue and water solutions were completely separated (Figure 2-4a-1) and the intensity curve was similar to a step function (Figure 2-4b-1). Moving along the length of the channel at each velocity setting, the *SI* decreased gradually as a result of Dean flow-based recirculation of fluids in the channel (Figure 2-4a-2 and 2-4b-2). The minimum SI value in each plot was obtained when the water stream was completely sandwiched in between two methylene blue streams at its top and bottom sides (Figure 2-4a-3). This condition resulted in a flat intensity diagram (Figure 2-4b-3) and minimization of σ in Equation 7. Afterwards, the *SI* started increasing to its first peak value due to continuation of fluids recirculation that resulted in separation of methylene blue and water solutions into two phases in the radial direction of the channel again (180° recirculation in Figure 2-4a-4 and Figure 2-4b-4). The peak SI value was not equal to the initial unity because of two reasons; first, minor diffusion taking place along the interface of water and methylene blue solutions and second, various fluid particles assuming different local Dean velocities at different locations along the cross section of the channel. These factors prevented achieving a complete switch in fluids' position with an interface as distinct as the one at the channel entrance. They led to an overall reduction of c_i and $\bar{c}$ values in Equation 7 at the location of the switch, hence a smaller *SI* value in Equation 8. Although these factors resulted in reduction of *SI* at the first peak, but the switching location (L_s) could still be determined from the *SI* plot which was later used to calculate the average Dean velocity in the channel. By moving further downstream in the channel, fluid recirculation continued to occur and dependent on the fluid velocity, the *SI* curves

either demonstrated a second peak corresponding to a second switch of position or a plateau that indicated indistinguishable mixing of fluid layers in the channel.[46,55]

As mentioned above, the first peak on the SI diagrams corresponded to the exact switching location of methylene blue and water solutions in the channel which is denoted by the switching length, L_s, in Figure 2-5. With increasing the axial velocity of the fluid from 0.15 $m.s^{-1}$ to 0.74 $m.s^{-1}$ (De=2.73-6.82), we clearly observed that the fluid recirculation became stronger and the SI peaks started to shift towards the left of the diagrams corresponding to reduction of switching length from L_s=9 cm (at V_x=0.15 $m.s^{-1}$) to L_s=2.4 cm (at V_x=0.74 $m.s^{-1}$). We used the switching length L_s and the corresponding axial velocity V_x to calculate the time of the first switch ($t=L_s/V_x$). We also identified appearance of a second switch (i.e., complete 360° recirculation at the 2nd peak on SI diagrams in Figure 2-5e) as the axial velocity was increased in the channel to 0.59 $m.s^{-1}$ and beyond. This was because the vortices got stronger at higher De numbers and switching length decreased resulting in an opportunity for the fluids to show a complete recirculation in the device. Further switches were not identifiable with our quantitative *SI*-based approach either due to full mixing of the fluids or enhanced 3D complexity in layered structure of the fluids that could no longer be distinguished with our top view-based imaging method.

2.3.3 Estimation of Average Lateral Travel Distance and Dean Velocity

To approximate the average Dean velocity (V_{De}) from the experiments discussed in the previous section, an estimation of the average lateral travel distance by the fluid particles (L_R) was needed. In this case, V_{De} can be calculated from Equation 9 using the experimentally determined switching time in the previous section.

$$V_{De} = \frac{L_R}{t} = \frac{L_R V_x}{L_s} \quad (9)$$

The average lateral travel distance was approximated at 0.75D by Ookawara et.al[67] by assuming an simplified rectangular streamline shape for Dean vortices. However, Martel and Toner[34] showed that the channel curvature ratio ($\delta = \frac{D}{2R}$) is a key parameter for determination of the shape of Dean vortices. Their simulations (confirmed by our numerical results) indicated that for curvature ratios smaller than 0.008, fluid particles tend to follow elliptical streamlines such as the one shown in Figure 2-6a. However, for δ values greater than 0.008, the bulk of the laterally-flowing fluid shifts towards the outer wall of the channel, leading to formation of asymmetric oval shape streamlines for Dean vortices. Hence, the fluid elements closer to the inner wall of the channel participate less in the circulatory motion. Accordingly, we approximated our Dean vortices with elliptical shape streamlines at low δ (<0.008 in Figure 2-6a), while a half-circle half-ellipse shape (Figure 2-6b) was used to approximate the lateral travel distance, L_R, of fluids in channels with higher curvature ratios (δ>0.008). Average Dean velocities for the experiments presented in Figure 2-6 were then calculated based on Equation 9 using the approximated L_R values discussed above and the results are presented in Figure 2-6c.

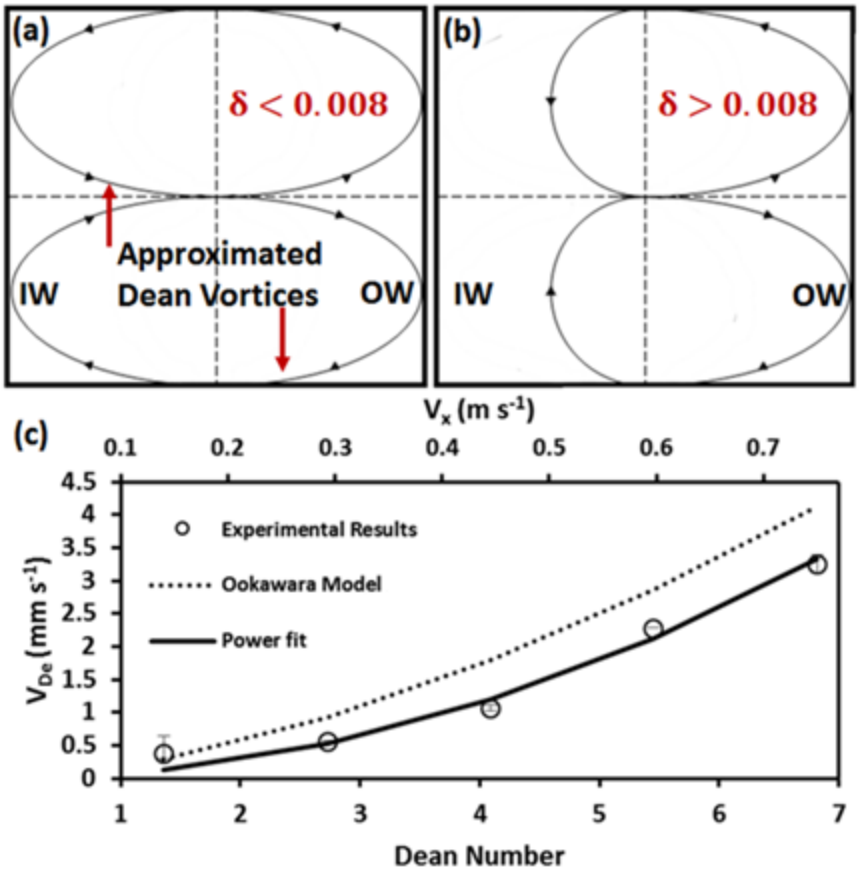

Figure 2-6. Dean vortex shape approximation and calculated average Dean velocities in a curved microchannel with R=2 cm and cross section area of 150µm×150µm. Dean vortices were assumed to follow (a) an elliptical path for δ<0.008 ($\delta = D/2R$) and (b) a half-elliptical half-circular path for δ >0.008[34]. (c) The switching lengths obtained experimentally and the approximated average lateral travel distances were used to calculate the average Dean velocities (V_{De}) at different axial velocities in the abovementioned device. The solid line in (c) shows a power function ($V_{De}=aDe^b$) fitted over the experimental data points with constants a=0.072 and b=2 (R^2=0.98). The dashed line in (c) shows the Ookawara's[67] equation for Dean velocity (mm.s^{-1}) with a=0.18 and b=1.63 (R^2= 0.71).

As demonstrated in Figure 2-6c, for a curved microchannel with R=2 cm and cross section of 150µm×150µm (elliptical streamline model with $\delta = 0.0038$), by increasing the axial velocity of the fluid from 0.15 m.s^{-1} to 0.74 m.s^{-1}, the average Dean velocity increased from V_{De}=0.57 mm.s^{-1} to V_{De}=3.25 mm.s^{-1}, respectively. This clearly supports the discussion of faster switching of fluids at higher De numbers in a curved microchannel. Following the proposed power equation type ($V_{De}=aDe^b$) by Ookawara et al.[67], we fitted a power function to our calculated V_{De} values in Figure 2-6c. The experimentally-driven

constants of the fitted equation were *a=0.072* and *b=2* (R^2*=0.98*) which were different from the numerical values reported by Ookwara et.al[67] (i.e. *a=0.18* and *b=1.63*, R^2*=0.71*). The power dependence of V_{De} on the Dean number has been confirmed by others[34] while the disagreement between Ookawara's equation and case-specific models has been reported by researchers such as Guan et.al.[85] These differences may be originated from differences in fluid properties and or dimensional variations among different microchannels. Having shown that our methodology has the capability of characterizing the average Dean velocity in a curved microchannel, we continued our investigations by examining the effects of other important parameters such as the radius of curvature, hydraulic diameter, width, height, and viscosity on Dean velocity using a combination of complementary experimental and numerical approaches. The objective of these parametric studies was to explore if an inclusive equation could be proposed for estimation of average Dean velocity in curved microfluidic channels.

2.3.4 Effect of Channel Radius of Curvature on Dean Velocity

Here, we examined the effect of the radius of curvature of the microchannel on Dean velocity. For this purpose, curved microchannels with the same cross section area of 150µm×150µm but various radii of curvature of R=0.5, 1, 1.5, and 2cm were fabricated and tested at various axial flow velocities (V_x=0.15-0.74 $m.s^{-1}$). The results of this study are shown in Figure 2-7a. As demonstrated, at a constant axial velocity, an increase in the radius of curvature resulted in reduction of Dean velocity due to lowering of the Dean vortex strength. The effect of radius of curvature was more strongly observed at higher axial velocities. We also plotted the obtained V_{De} values in the above set of experiments as a function of Dean number in Figure 2-7b.

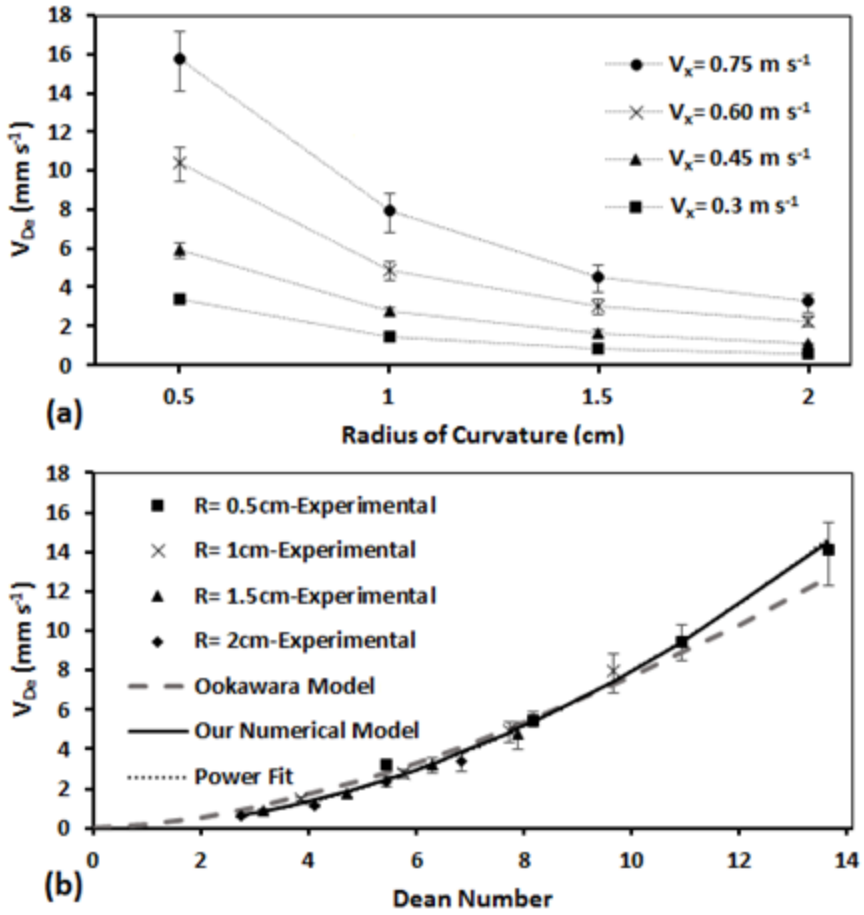

Figure 2-7. Effect of radius of curvature of the channel (R=0.5-2cm) on Dean velocity shown (a) at various axial velocities and (b) using the non-dimensional Dean number for devices with 150µm×150µm cross section. The Dean velocity decreases as the radius of curvature increases at each inlet velocity. Increasing the Dean number (via axial velocity) for each device resulted in an increase in Dean velocity. A power function ($V_{De}=aDe^b$) fitted over the experimental results in (b) provided the constants of a=0.090 and b=1.95 with R^2=0.98. Numerical results based on our model (a=0.096 and b=1.92) and Ookawara's model (a=0.18 and b=1.63) are also shown with a solid and a dashed line, respectively.

For devices that had different radii of curvatures but approximately the same Dean number, we observed a highly similar Dean velocity as shown in Figure 2-7b. A power function ($V_{De}=aDe^b$) was fitted to the overall results in Figure 2-7b (dotted line) and the correlating constants of $a=0.090$ and $b=1.95$ ($R^2=0.98$) were obtained. The Dean velocities from devices with various radius of curvature followed this power correlation precisely, indicating that the effect of radius of curvature is sufficiently captured by the R-parameter already included in the De number. For comparison purposes, the Ookawara's

equation is also plotted in Figure 2-7b (dashed line). With a R^2 value of 0.94, it overpredicted the experimental Dean velocities at De<8 and underestimated them at higher De values. We hypothesize that the mismatch between Ookwara's equation and our experimental results in Figure 2-6c and 2-7b might stem from the differences between the geometrical dimensions of the curved microchannels and approximated lateral travel distances used in both studies. Therefore, we decided to develop and validate a numerical model to further investigate the effect of other parameters on Dean velocity.

2.3.5 Numerical Model to Investigate Dean Velocity Parametrically

As discussed in the Methods section, we used COMSOL Multiphysics to simulate the Dean flow in our microchannels and obtain the Dean velocities accordingly. The experimental conditions reported in Figure 2-7b were simulated and the numerical results are plotted with a solid black line in Figure 2-7b for comparison purposes. The results followed a power function trend (R^2=0.98) with *a* and *b* coefficients of 0.096 and 1.92, respectively, that were slightly different from the power function fit to our experimental results. This confirmed that our model could predict Dean velocities with a better precision when compared to the model reported by Ookawara et.al.[67] This better precision stems from higher similarity between our numerical simulation and experiments in terms of geometry and flow conditions as well as a better approximation for lateral travel distance of fluid particles as shown in Figure 2-6(a-b).

The power functions reported in this paper[67] and by other researchers for estimation of Dean velocity are limited solely to parameters involved in the Dean number with fixed powers. We hypothesized that factors such as specific channel geometries (i.e. width vs. height) and fluid viscosity may have significant effects on Dean velocity that available

power functions cannot predict accurately. To investigate this, we used our validated numerical model to examine the effect of these parameters on Dean velocity.

2.3.6.1 Effect of Hydraulic Diameter on Dean Velocity

The effect of hydraulic diameter of the channel (D) on Dean velocity is captured by a power of 2.88 in our preliminary model presented in previous section ($V_{De}=aDe^{b}$, $a=0.096$ and $b=1.92$). Here, we were interested to investigate whether this power sufficiently captures the effect of hydraulic diameter on Dean velocity. For this purpose, we performed simulations on square cross-section microchannels with R=0.5 cm and hydraulic diameters of 100µm-300µm at 0<De<30. We already showed in Figure 2-7b that at a constant De number, the radius of curvature does not affect Dean velocity significantly. Hence, the smallest radius of curvature was selected for numerical investigations of hydraulic diameter which reduced the number of mesh elements and time of computation considerably. Results of these simulations are presented in Figure 2-8a. As demonstrated, at a constant axial velocity, an increase in the hydraulic diameter of the channel resulted in an incease in the Dean velocity due to stronger secondary vortices (i.e. higher De numbers). The resulted Dean velocities in the numerical simulations above were also plotted as a function of Dean number in Figure 2-8b.

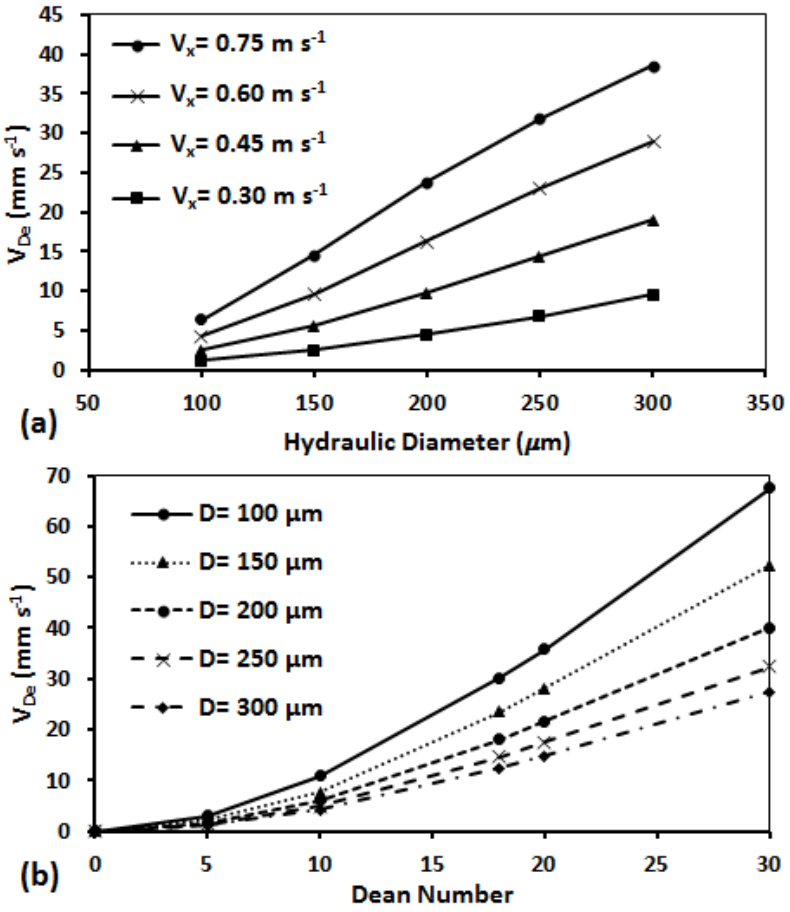

Figure 2-8. Effect of channel hydraulic diameter (D) on average Dean Velocity (V_{De}) using numerical modeling of a curved microchannel with R=0.5cm radius of curvature shown (a) at various axial velocities and (b) using the non-dimensional Dean number. At each inlet velocity, increasing the hydraulic diameter resulted in higher V_{De}. But when plotted V_{De} as a function of De in (b), we observed that the hydraulic diameter inversely affects the V_{De} when Dean number is kept constant. Single a and b constants could not be found to predict V_{De} with a single power function ($V_{De}=aDe^b$).

As shown in Figure 2-8b, when De number increases at a constant hydraulic diameter, the Dean velocity also increases due to formation of stronger secondary vortices. The results followed a power function ($V_{De}=aDe^b$) similar to what we observed in Figure 2-6c and 2-7b. However, a single power function with the same coefficients *a* and *b* could not be fitted over all the data points, suggesting that the hydraulic diameter parameter with a fixed power could not thoroughly capture the effect of channel geometry on Dean velocity. In other words, increasing the hydraulic diameter while keeping the De number constant resulted in reduction of the Dean velocity which completely contradicts with predictions

provided by the power functions presented above or used in various forms in the literature. The hydraulic diameter is derived from the width and height of the channel. Hence, to further investigate the effect of channel geometry on Dean velocity, we continued our studies with modeling of a series of channels with different widths and heights in the following section.

2.3.6.2 Effect of Channel Width and Height on Dean Velocity

The effect of channel geometry was further investigated by examining the roles of width (w) and height (h) of the channel individually on Dean velocity. Our strategy was to simulate 0.5 cm radius of curvature curved microchannels with square and rectangular cross sections that had widths and heights of 100 μm, 150 μm and 300 μm. The resultant Dean velocities for different combinations of channel widths and heights at various De numbers are plotted in Figure 2-9.

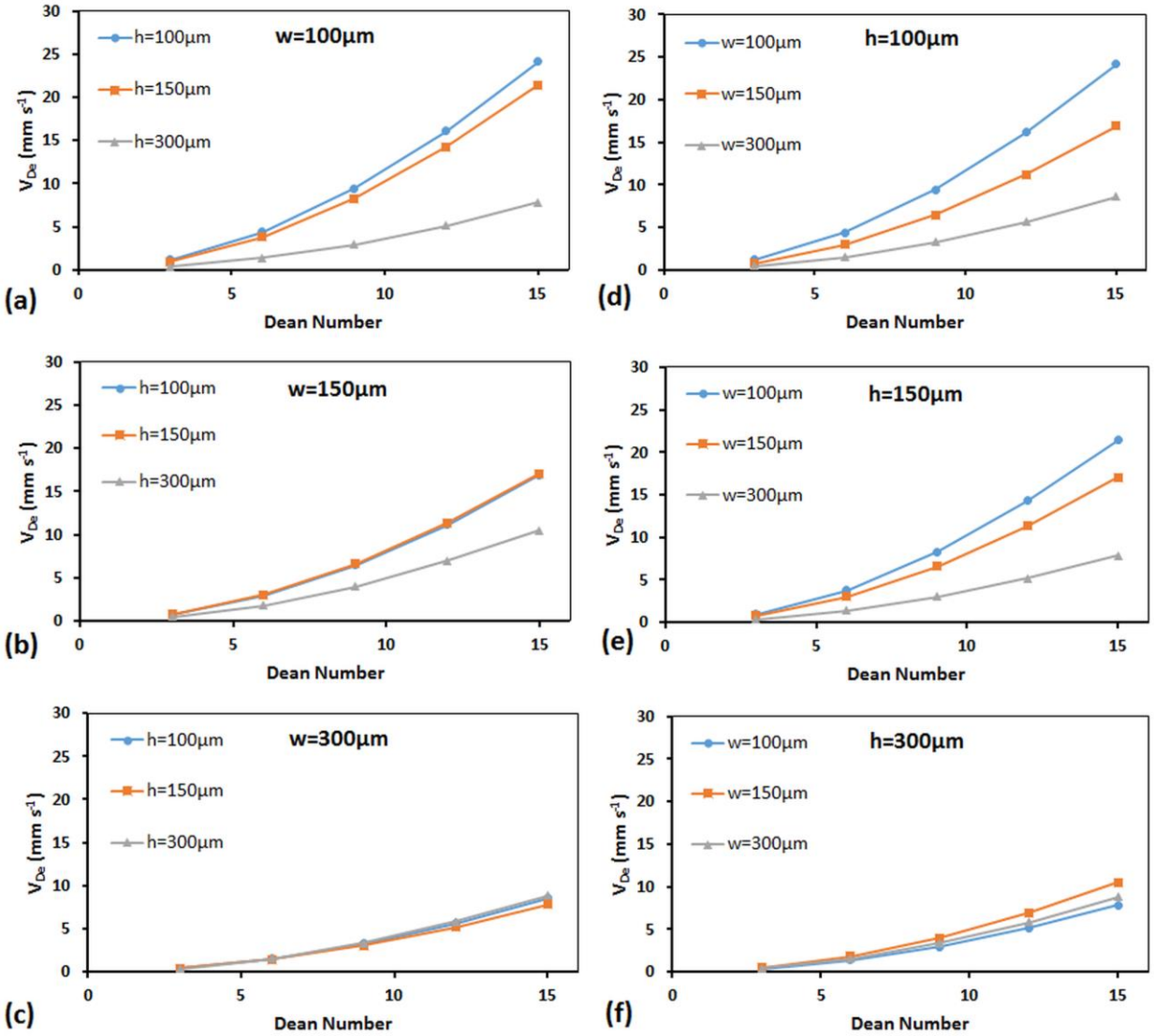

Figure 2-9. Effect of channel width (w) and height (h) on Dean velocity for curved microchannels with R=0.5 cm. (a-c) show the effect of height at fixed channel widths while (d-f) show the effect of width at fixed channel heights on Dean velocity.

As shown in all plots of Figure 2-9, increasing the De number at a constant channel width and height expectedly resulted in an increase of Dean velocity. At a constant De number, both height and width had an inverse effect on Dean velocity as shown in Figure 2-9(a-c) and Figure 2-9(d-f), respectively. For instance, increase of channel height from 100 µm to 150 µm to 300 µm at a constant w=100 µm (Figure 2-9a) and De=15 resulted in a decrease of Dean velocity from V_{De}=24.2 mm.s^{-1} to V_{De}=21.5 mm.s^{-1} to V_{De}=7.8 mm.s^{-1},

respectively. This is because at a constant w, the higher h corresponds to a longer distance that fluid elements should travel in a vortical motion, which results in a lower V_{De}. However, as the width of the channel became larger, the effect of height on Dean velocity became less dominant. For example, in the 300µm-wide microchannel (Figure 2-9c), changes in height did not significantly affect Dean velocity at any constant De number. Similar trends described above for height were also seen for the effect of width of the channel on Dean velocity as demonstrated in Figure 2-9(d-f). Increase of width at a constant height decreased the Dean velocity when De number was maintained constant. However, this decreasing trend became less significant as the height of the channel increased from h=100µm (Figure 2-9d) to h=300µm (Figure 2-9f).

The overall behavior can be explained by introducing the larger dimension of the channel as the determinative parameter influencing the Dean velocity. Channels with equal larger dimension possessed Dean velocities very close to each other and variation in the smaller dimension of the channel had low to no effect on the Dean velocity in all cases. This makes a logical sense because the larger dimension of the channel determines the distance along which fluid particles must travel mostly with their assumed Dean velocities. The results of this section suggested that an additional factor representing the inverse effect of the largest dimension of the microchannel on the Dean velocity must be included in the comprehensive correlation that we aim to derive for V_{De}.

2.3.6.3 Effect of Kinematic Viscosity on Dean Velocity

Having studied the effects of various channel geometries on Dean velocity, we became interested in investigating whether the kinematic viscosity parameter in the De number is sufficient to capture the effect of this variable on Dean velocity. In other words, we wanted

to understand if changing the viscosity while keeping the De number constant results in any change in the Dean velocity. Therefore, using our numerical model we simulated a microfluidic device with R=0.5 cm radius of curvature and cross-sectional dimension of 150µm×150µm. We increased the kinematic viscosity of the fluids from $\nu = 10^{-6}$ m^2.s^{-1} to $\nu = 3.21 \times 10^{-6}$ m^2.s^{-1} corresponding to 0-50% volumetric water-glycerol mixtures based on the results of Cheng.[83] Results of these simulations are presented in Figure 2-10a. As demonstrated, at a constant axial velocity, an increase in the viscosity of the fluid resulted in reduction of the Dean velocity due to weakening of the secondary vortices (i.e. lower De numbers). Dean velocities as a function of De number are also plotted in Figure 2-10b for the above experiments.

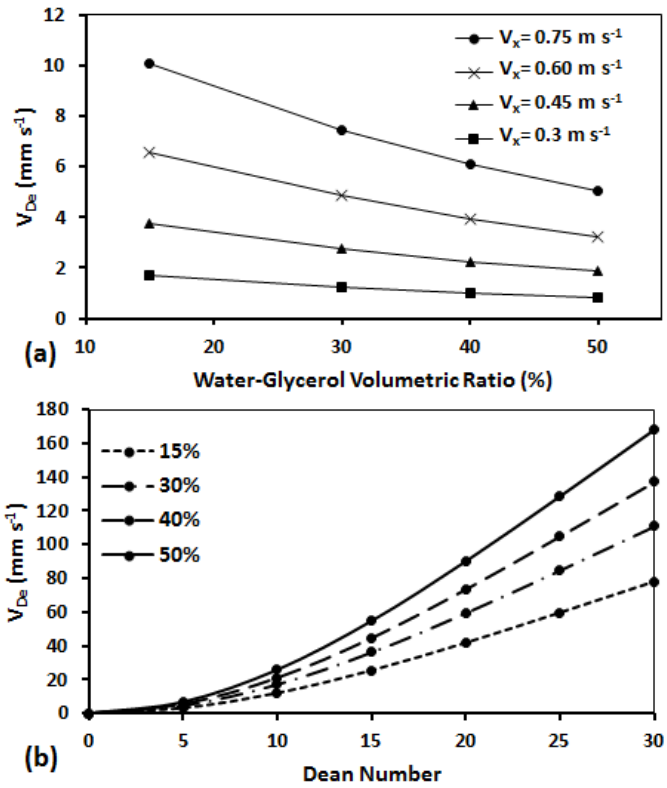

Figure 2-10. Effect of fluid kinematic viscosity on Dean velocity in a 150µm×150µm curved microchannel with R=0.5 cm shown (a) at various axial velocities and (b) using the non-dimensional Dean number. Increasing the viscosity while axial velocity is constant caused a reduction in V_{De}. However, when Dean number was kept constant, viscosity directly affected the V_{De}. Single a and b constants could not be found to predict V_{De} with a single power function ($V_{De}=aDe^b$).

As shown in Figure 2-10b, an increase in the De number at each viscosity level causes the Dean velocity to increase by following a power function ($V_{De}=aDe^{b}$) as observed for other parameters above. However, two fixed values for *a* and *b* could not be found to represent all data points with a single power function. Thus, we concluded that the effect of kinematic viscosity should be included further in the final correlation that we aim to derive for V_{De}.

2.3.7 Non-Dimensional Dean Velocity Correlation

Our experimental and numerical results in the previous sections along with other researchers' work has led us to conclude that Dean velocity has a power-function dependency on the De number. However, the existing functions presented in the form of $V_{De}=aDe^{b}$ are not able to represent the effect of some parameters such as the largest channel dimension (s) at all, while not sufficiently capable of capturing the effect of some other parameters such as kinematic viscosity (υ). Here, we propose that these parameters should be added to the above formula (i.e. Equation 10) in order to obtain a more comprehensive correlation for estimation of Dean velocity in curved microchannels.

$$V_{De} = a(\frac{\nu}{s})^{n} De^{b} \tag{10}$$

where *a*, *b* and *n* are the correlation constants that were needed to be determined. In order to find these unknowns, Dean velocities as a function of $\left(\frac{\nu}{s}\right)^{n} De^{b}$ were plotted using all of our numerical results presented before (Figure 2-11). The *n* and *b* values were varied in the range of 0.25-2.5 and the best fits to our data points were investigated. As seen, the lowest dispersity of the data points was observed in the case of n=1 and b=1.63.

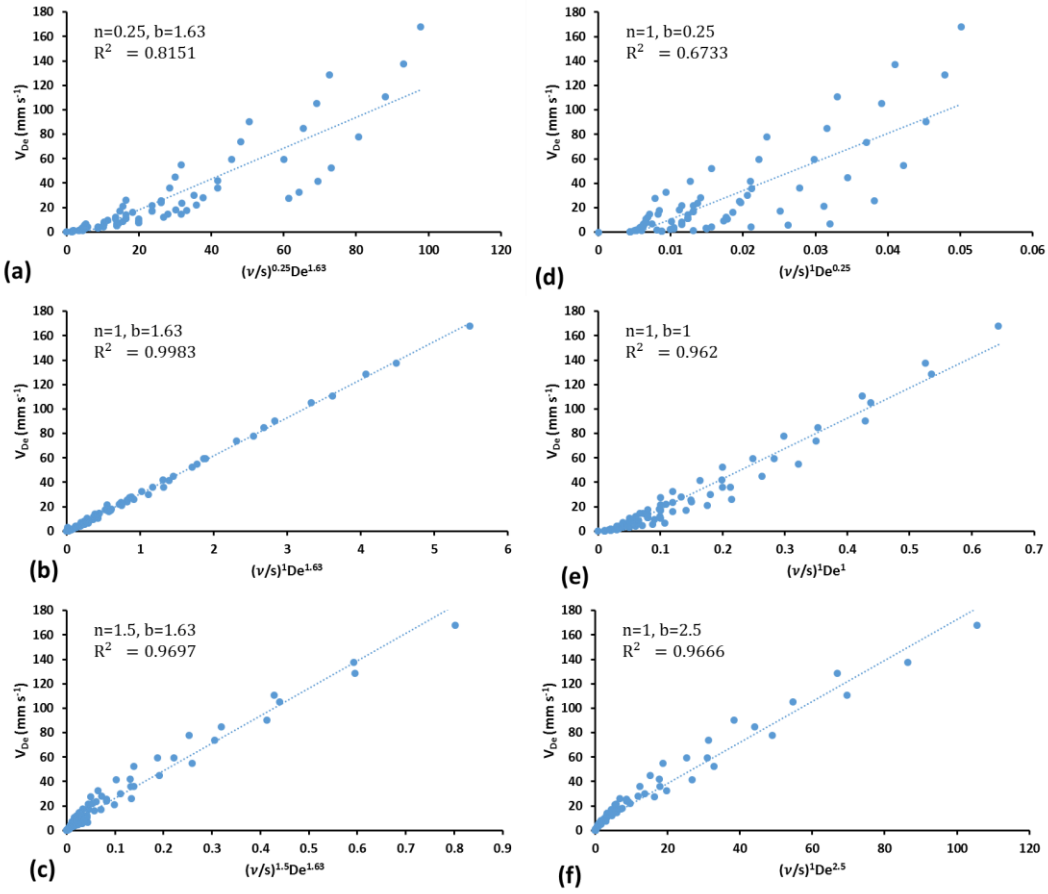

Figure 2-11. Dean velocity plotted against $\left(\frac{\nu}{s}\right)^{n} De^{b}$ *based on all numerical and experimental results obtained in this study. (a-c)The magnitude of b was set to 1.63 for similarity in De power to the commonly used value in the literature while n was varied from 0.25 to 2.5 to obtain the best fit (i.e. n=1). (d-f) Superiority of b=1.63 was tested by setting n=1 (concluded from a-c) and changing b from 0.25 to 2.5*

In order to quantitatively prove the appropriateness of n=1 and b=1.63 values, we fitted a linear function over the data points. We calculated R^2 values for each case as a measure of how well the fitted function predicted the behavior of data points[86] (Figure 2-12). In general, a curve with higher R^2 can better capture the variance of the data points and is a better fit. Figure 2-12a. shows R^2 vs. b while n was kept constant (n=1). As seen, R^2 increases as b increases and reaches its peak at b=1.63 and drops afterwards. Similar behavior was seen when b was maintained constant at 1.63 and n was varied from 0.25 to 2.5 (Figure, 2-12b). The maximum acheivable R^2 value was at n=1.

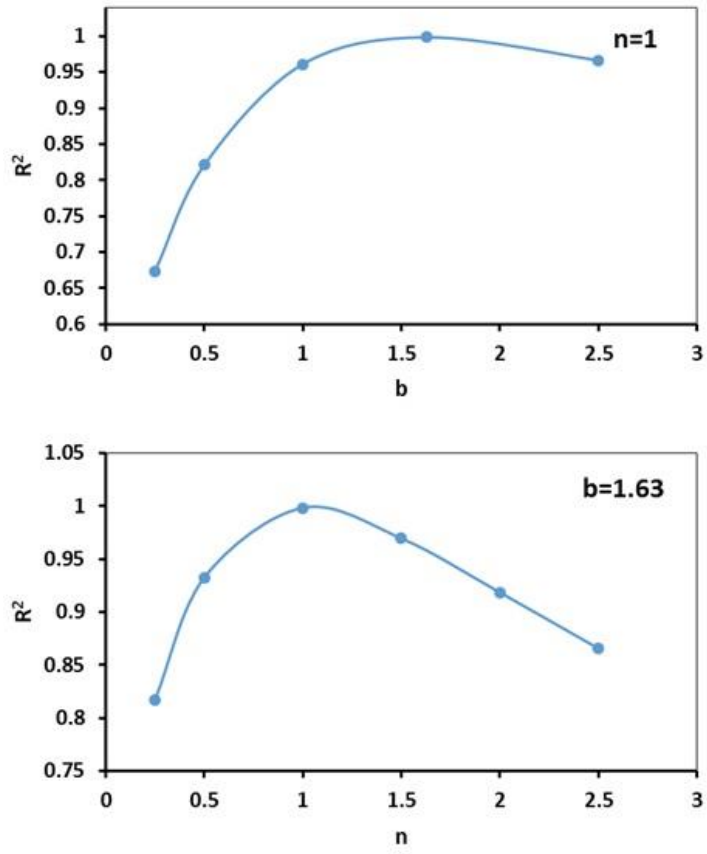

Figure 2-12. Values of R^2 for (a) constant n and b as the variable and (b) constant b and variable n. The maximum value for R^2 is seen for the case of n=1 and b=1.63.

Consequently, n=1 and b=1.63 were selected as the best coefficients that gave the highest R^2 value. Hence, by setting *n=1*, the numerical Dean velocities will become linearly dependent on $\left(\frac{\nu}{s}\right) \mathrm{De}^{1.63}$ with a constant of linearity of *a=0.031* as shown in Figure 2-13 (best fit with R^2=0.9982).

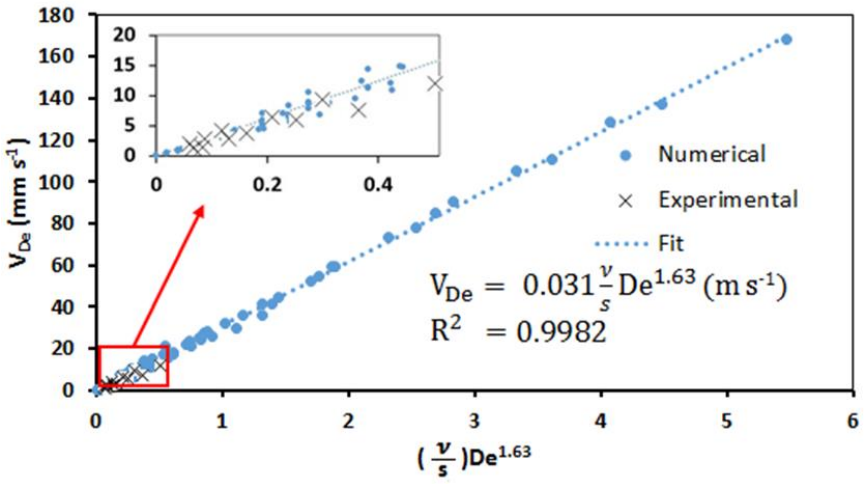

Figure 2-13. Dean velocity plotted against $\left(\frac{\nu}{s}\right) De^{1.63}$ based on all numerical results obtained in this study. A linear function could be fitted over the data points (R^2=0.9983) with a=0.031 as the constant of linearity. The inset figure shows our experimental Dean velocities from single experiments in two devices with cross sectional dimensions of 100µm×150µm and 300µm×150µm (cross data points) that follow the numerically-determined fit very well.

Based on the studies above, the final correlation for the average Dean velocity in a curved microchannel can be presented as:

$$V_{De} = 0.031 \left(\frac{\nu}{s}\right) De^{1.63} \tag{11}$$

Equation 11 can be rearranged to provide a fully dimensionless relationship between Reynolds number based on average Dean velocity and largest dimension of the channel (called lateral Re number) and the De number based on axial velocity.

$$Re_{s,V_{De}} = 0.031\ De^{1.63} \tag{12}$$

Lastly, the suitability of the proposed correlation was experimentally validated. For this purpose, we conducted a new set of experiments in devices with R=1 cm and cross-sectional dimensions of 100µm×150µm and 300µm×150µm. We also conducted experiments with a 15% volumetric water-glycerol mixture in a device with R=0.5 cm and cross-sectional dimension of 150µm×150µm . The resultant experimental Dean velocities are plotted in the inset of Figure 2-13. As shown, the proposed correlation in Equation 12

was accurate enough for estimation of Dean velocities in these experiments.

2.4 Conclusion

In this chapter, we developed experimental and numerical models to examine the effects of radius of curvature, hydraulic diameter, and width and height of the channel as well as the kinematic viscosity of the fluid on Dean velocity in curved microchannels. We showed that Dean velocity cannot be merely estimated with a widely-used power function ($V_{De}=aDe^{b}$) because this correlation fails to predict the effects of the larger dimension of the channel and kinematic viscosity on Dean velocity. Instead, we proposed a semi-empirical correlation that relates the lateral Reynolds number of the channel (based on V_{De} and the largest channel dimension) to the Dean number. This correlation was accurate enough to predict the average Dean velocity for Dean numbers lower than 30 for various experimental conditions. We envision the widespread use of this correlation in estimation of Dean velocities in curved and spiral microchannels used widely in sample processing and preparation applications.

Chapter 3

Solution Exchange of Microparticles in Curved Microchannels[2]

3.1 Introduction

As discussed in Chapter 1 of the thesis, sorting of suspended particles in a medium and exchanging their solution to another fluid is of paramount importance in sample preparation that is a major step in biological applications. Many attempts have been made to integrate various steps of sample preparation on Lab on a Chip devices. However, solution transfer of particles has not been studied extensively and current methods are often limited with low throughputs and particle handling concentrations. In this chapter, a novel method is proposed as a means of transferring suspended particles in a solution to another passively inside a curved microchannel discussed in the previous chapter. For this purpose, fluid switching behavior of co-laminar flows due to the presence of secondary flows in curved channels (described in chapter 2) along with particles focusing caused by inertial and Dean drag forces will be investigated both analytically and experimentally. We anticipated to achieve solution exchange at high flow rates of 1 $ml.min^{-1}$ and higher by manipulating the switching location of carrier and buffer solutions.

[2] A version of this chapter is submitted to Analytical Chemistry journal. P. Bayat and P. Rezai, Anal. Chem, 2017, submitted.

3.2 Materials and Methods

3.2.1 Particle and Bacteria Suspension Preparation

Microparticles with diameters of 19 μm (CM-200-10, 18-22.9 μm with a peak at 18.8 μm), 11 μm (CM-100-10, 10-13.9 μm with a peak at 10.8 μm), and 4 μm (CM-40-10, 4-4.5 μm with a peak at 4.37 μm) were purchased from Spherotech Inc. (IL, USA). The 11 μm or 4 μm microparticle solutions with concentration of 10^6 particle.mL^{-1} and 19 μm microparticle solutions with concentration of 10^5 particle.mL^{-1} were prepared in 10% Trypan blue (Sigma Aldrich, MO, USA) dyed deionized (DI) water for the single-particle experiments. The concentration of 11 μm particles was reduced to half for the duplex experiments with 4 μm particles. Tween 20 (Sigma Aldrich, MO, USA) at 1% w/v was added to the solutions to avoid any potential aggregation of microparticles. DI water was used as the target fluid in all particle-based experiments.

Ampicillin-resistant *E. coli* K12 ER2420/pACYC177 bacteria were picked from a plate colony and grown overnight in LB broth (Miller) media purchased from Sigma Aldrich (Mo, USA) and on a shaker incubator at 37℃ and 200 rpm. Microparticles with 19 μm diameter (as surrogates for cells or embryos) with a concentration of 10^5 particle.mL^{-1} were then spiked in the bacterial suspension. The mixture of *E. coli* and particles served as the carrier fluid suspension while phosphate buffer saline (1x PBS) was used as the target fluid.

3.2.2 Microfluidic Centrifuge Device and Experimental Setup

The microfluidic centrifuge device (Figure 3-1a) consisted of a 180° section of a curved microchannel with radius of curvature of R=1.185 cm and cross-sectional dimension of 300μm×60μm. Two inlet channels were embedded at the beginning of the curved section

with equal widths of 150 µm for insertion of carrier and target fluids into the device. The inner outlet was 100 µm wide while the outer outlet was 200 µm. A straight channel was added at the end of the curved channel with the length of 0.5 cm to let the fluids recover after experiencing the Dean flow[55]. Two 10 mL syringes containing the solution of microparticles in 10% Trypan Blue and DI water were connected to a syringe pump (Legato 110, KD Scientific, USA) to deliver the fluids into the channel at a flow rate of 1 $mL.min^{-1}$.

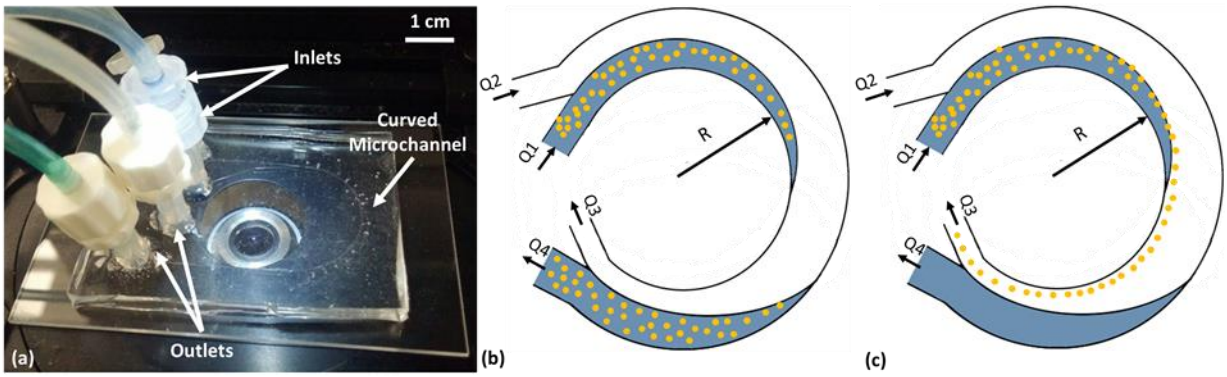

Figure 3-1. (a) The microfluidic device used for solution exchange microparticles that included two inlets, two outlets, and an R=1.185 cm curved microchannel (b) Microparticles do not focus when Dean drag is the dominant force. Dean vortices are strong enough to carry the microparticles to the outer outlet. (c) Inertial focusing of microparticles when the inertial force is dominant. Inertial force tends to focus the microparticles close to the inner wall. Higher R_f values cause the focusing stream to be narrower.

The microfluidic device was fabricated using soft lithography[87]. The master replication mold was made by spinning SU8 2035 photoresist (Microchem Corp., MA, USA) over 4 in diameter silicon wafers (Wafer World Inc., FL, USA). Next, pre-bake treatment was conducted at 65℃ and 95℃ followed by exposure to ultraviolet light through a photomask. The wafer was then post-baked at 65℃ and 95℃ and developed in SU8 developer solution to dissolve the unexposed photoresist. Eventually, the wafer was hard-baked at 140℃. Polydimethylsiloxane (PDMS, Sylgard 184 silicone elastomer kit, Dow Corning) was then mixed in 10:1 base:agent ratio, casted on the master mold, and bonded to a

glass slide using an oxygen plasma machine (Harrick Plasma, PDC-001, NY, USA). Tubes were installed in place and experiments were conducted under an inverted microscope (Leica, Wetzlar, Germany).

3.2.3 Data analysis

The quality of particle focusing was measured by counting the number of microparticles in collected samples from the outlets and the initial solution using a hemocytometer (Marienfeld, Lauda-Königshofen, Germany). The particle sizes were distinct enough to be easily distinguishable from each other in a high magnification microscopic image. Particle sorting efficiency between the two outlets was defined as the number of particles in the target outlet divided by the total number of collected particles. Particle recovery rate was defined as the percentile ratio of the total number of collected microparticles to the number of microparticles in the initial solution. The purity of separation for duplex experiments was reported as the number of target particles in each outlet divided by the total number of collected particles in that outlet.

The purity of solution exchange, related to concentration of Trypan blue in the fluids, was measured by spectrophotometry. A standard calibration curve was established by measuring the absorbance of 0-100% Trypan blue dye in water at 607nm with a spectrophotometer (Shimadzu UV2600, Japan). The absorbance of the collected sample from the inner outlet was then measured and compared with the standard curve to determine the percentage concentration of Trypan blue contaminant (C_{TB}) in the target outlet. The purity of solution exchange was defined as 100-C_{TB} in the inner outlet.

In order to calculate the bacteria separation efficiency from microparticle surrogates, colony forming units were counted after plating serial dilutions of the collected samples

from the outlets on ampicillin-doped LB-agar plates incubated at 37℃. Bacteria separation efficiency was measured by calculating the percentage of *E. coli* in each outlet.

3.3 Theory

Particle manipulation requires determining the dominance of the forces that a particle experiences in a curved microchannel. Two forces, namely Dean drag and inertial forces, are known as the main forces that define the focusing location of microparticles[40]. Dean drag leads to recirculation of microparticles over the cross-section of the channel. It is assumed that Dean drag follows the Stokes' law and can be expressed as shown in Equation 13.

$$F_D = 3\pi\mu a V_{De} \tag{13}$$

Here, μ [Pa.s] and a [m] are dynamic viscosity of the fluid and diameter of the microparticle. The Dean velocity in Equation 11 can be used to calculate the Dean drag force on a microparticle in a curved microchannel. The net inertial force (F_L) consists of shear gradient and wall induced forces (Equation 1 and 2). F_L is defined in Equation 14 where ρ [kg.m^{-3}] shows the density of the fluid, G is defined as the shear rate ($G=U_{max}/D$, where D [m] is the hydraulic diameter of the channel and $U_{max}=1.5U_{avg}$).

$$F_L = \rho G^2 C_L a^4 \tag{14}$$

The ratio of the inertial force to the Dean drag force is shown by R_f (Equation 15) and can be used as a quantitative index to identify whether focusing happens in a microchannel or not. As a rule of thumb, $R_f \gg 1$ results in inertial focusing while $R_f \ll 1$ defines dominance of the Dean drag[66]. Microparticles in the Dean drag regime recirculate along the channel cross section by following the Dean vortices (Figure 3-1b) while microparticles with R_f

values of higher than 1 focus close to the inner wall of the channel due to the dominant inertial forces (Figure 3-1c). Increasing the R_f value results in narrowing the focusing stream.

$$R_f = \frac{F_L}{F_D} = \frac{\rho G^2 C_L a^3}{3\pi\mu V_{De}} \quad (15)$$

3.4 Results and Discussion

3.4.1 Design and Operation of the Microfluidic Centrifuge Device

We aimed to develop a device with the potential of separation of bacteria from larger particles, cells and embryos at high flow rates and their simultaneous washing into a clean buffer. For this purpose, we designed a curved microchannel with two inlets and two outlets (Figure 3-1a) to manipulate the carrier and target fluids with spiked particles in them as shown in Figure 3-1b and 3-1c. We used 4 µm microparticles as surrogates for bacteria and 11µm or 19 µm microparticles as surrogates for larger cells and embryos. Our target application required that the inner-inlet carrier fluid be moved to the outer wall of the channel to exchange its position with the outer-inlet target fluid. The smaller particles (e.g. bacteria) were desired to be maintained within the carrier fluid and the larger particles were needed to be inertially focused at the inner wall of the channel to become separated from the smaller particles while washed and concentrated into the target fluid simultaneously.

We first employed Equation 11 to design a curved microchannel that is capable of switching the radial location of the fluids at a flow rate of $Q_1 = Q_2 \approx 1$ mL.min^{-1} that is 10 times higher than the working flow rate of the currently available microfluidic solution exchangers. In conjunction with the other design criteria of putting small and large

particles under drag and inertia force dominances respectively (see below), our analysis resulted in a channel with cross-section dimensions of 300 µm×70 µm, length of 3.72 cm, and radius of curvature of 1.185 cm. Our fabricated device was equal in length and radius of curvature with the calculated dimensions. However, the channel height that we could microfabricate was ~60 µm.

Next, we evaluated our device theoretically, to ensure the thresholds of particle focusing at $Q_{total}=Q_1+Q_2=2$ mL.min^{-1}. We determined the strength of Dean drag and inertial forces that microparticles experience in our curved microchannel based on Equation 13 and Equation 14 as well as the R_f ratio in Equation 15. Based on these equations, inertial force scales with a^4 while Dean drag force is linearly proportional to particle diameter, a. Therefore, at low particle diameters, the Dean drag force dominates while inertial force prevails as the diameter increases. In order to figure out the dominance range for each force, we plotted the Dean drag and inertial forces versus the particle diameter in our device as shown in Figure 3-2. As depicted, microparticles with the diameter of 5.29 µm and less possess R_f values lower than 1 and theoretically lie in the Dean drag regime. R_f and the inertial forces dramatically increase as the diameter increases beyond 5.29 µm. Transition between the Dean drag and inertial regimes is not abrupt and there is a transition region where the forces are comparable and the microparticles are expected to be distributed all over the width of the channel. Particle focusing is not achievable for this case unless an external field, such as magnetic, is hypothetically employed or the geometry of the channel is altered. Determination of this transition regime needs further investigation and was beyond the scope of this thesis.

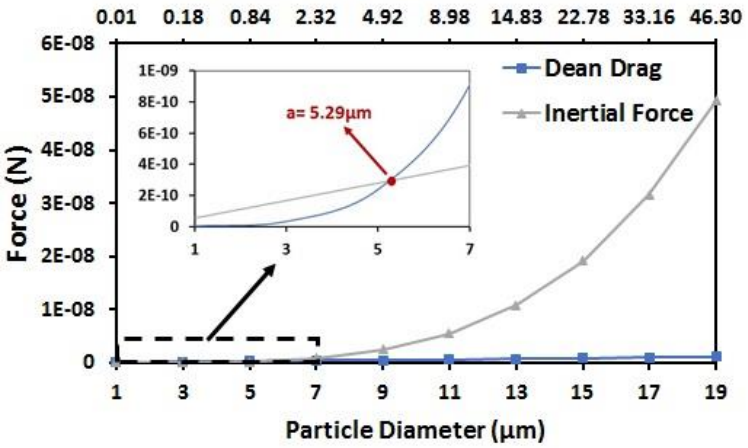

Figure 3-2. Theoretical magnitudes of Dean drag and inertial forces experienced by particles of various diameters, flown at Q= 1 mL.min^{-1} in the microfluidic centrifuge device. The R_f values corresponding to the particles are also shown on the secondary x axis (not to scale). At particle diameter of a=5.29 µm, the forces are equal and R_f=1. Particles with $a \gg 5.29$ µm fall in the inertial force dominance regime while for particles with $a \ll 5.29$ µm, Dean drag is the dominant force.

3.4.2 Behaviour of Single-Size Microparticles in the Device

We selected three microparticles with diameters of 4 µm, 11 µm, and 19 µm to experimentally evaluate our design criteria in the previous section for particle focusing and size-selective separation and solution exchange in our device. For this, we prepared three solutions of single sized microparticles in 10% Trypan blue and ran them through the device from the inner inlet. DI water was pumped into the outer inlet. Both flow rates were set to Q=1 mL.min^{-1} that was theoretically found to result in one complete switch of the fluids as described in the previous section. Based on the results in Figure 3-2, the 4 µm microparticles with R_f=0.56 were expected to get carried out with the carrier solution to the outer outlet (Figure 3-1b) while 11 µm (R_f=8.5) and 19 µm (R_f=45.6) particles were anticipated to focus close to the inner wall (Figure 3-1c). We performed the experiments three times for each particle size and calculated the number of microparticles in the collected samples from each outlet. The number of particles in each inlet and outlet, normalized with the number of particles in the initial sample, are shown in Figure 3-3.

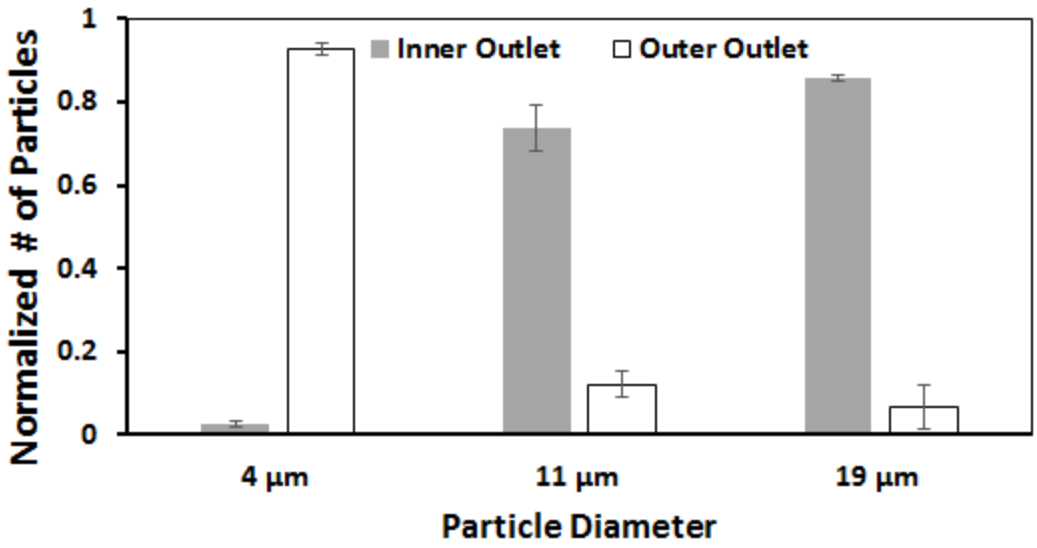

Figure 3-3. Number of microparticles in the inner outlet (gray columns) and the outer outlet (white columns) of the microfluidic centrifuge device, normalized by the number of microparticles in the initial sample, for 4, 11 and 19 µm microparticles tested one at a time in the device. The efficiency of retaining 4 µm particles in the carrier fluid, via the dominance of Dean drag forces, was 98±0.7%. The efficiency of inertial focusing and transferring of 11 µm or 19 µm particles to the target fluid was 86±2% and 93±0.7%, respectively. The recovery rate had the highest value of 95 ±1.2% for 4 µm and decreased to 86±8% for 11 µm and 92±5% for 19 µm particles.

As shown in Figure 3-3, 98±0.7% of 4 µm particles remained in the original carrier fluid due to the dominance of Dean drag forces and were extracted from the outer outlet. The recovery rate for this case was 95±1.2%. For 11 µm particles, the majority of the particles were inertially focused at the inner wall of the channel and collected from the inner outlet with the efficiency of 86±2% and recovery rate of 86±8%. The 19 µm particles had higher efficiency and recovery rate of 93±0.7% and 92±5%, respectively. The larger R_f value, which belongs to 19 µm particles, results in a stronger inertial force over Dean drag force, and a narrower focusing stream at the outlet of the device. Therefore, the width of focusing stream for 11 µm particles is larger than 19 µm particles. This causes more 11 µm particles to exit the device from the outer outlet, hence reducing the separation efficiency compared to 19 µm particles.

3.4.3 Solution Exchange and Separation of Two Microparticles in the Device

Next, we examined the capability of our device in performing simultaneous solution exchange of 11 µm particles and their separation from 4 µm particles in the outlet of the centrifuge device. For this purpose, we prepared duplex solutions of both particles and ran them into the microfluidic centrifuge with the same flow condition as mentioned above. The results in Figure 3-4 demonstrate that 11 µm particles successfully changed their solution from 10% trypan blue to DI water in the inner outlet (further discussed below) and got separated from 4 µm microparticles that were carried to the outer outlet. The purities of separation were 96±2% for 11 µm and 89±6% for 4 µm microparticles in the inner and outer outlets, respectively. These results demonstrate that the Dean drag-based transportation of 4 µm and inertia-based focusing of 11 µm particles are not affected in a duplex sample when compared to their counterpart singleplex behaviors discussed in the previous section.

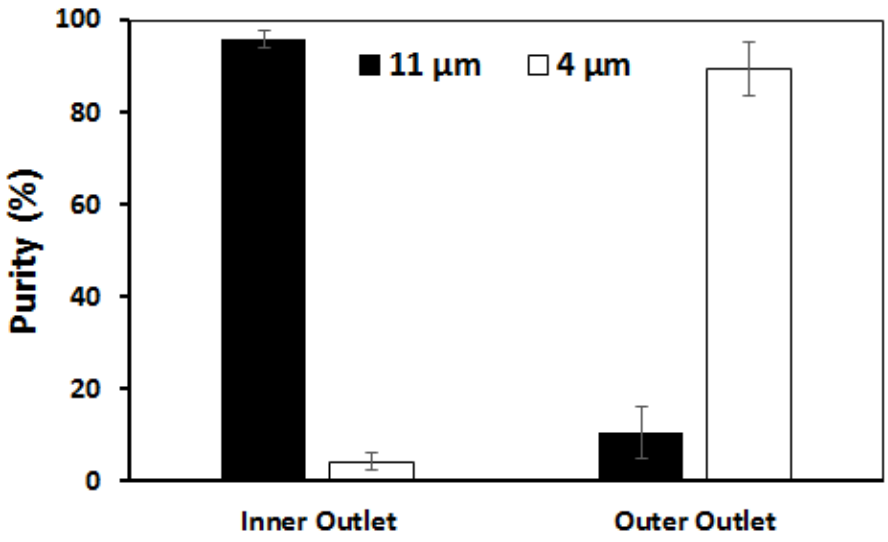

Figure 3-4. Separation purity reported as the percentile number of target microparticles divided by the total number of microparticles in each outlet. Separation purity was 96±2% and 89±6% in the inner and outer outlets, respectively.

Our aim was to wash the 11 µm particles from their original 10% trypan blue solution into

a clean buffer (called solution exchange), while they were being separated from the 4 µm particles in the device. The purity of solution exchange was defined as the concentration ratio of DI water in the collected sample from the inner outlet. The lower presence of trypan blue and higher percentage of DI water in the inner outlet shows a purer solution transfer for targeted 11 µm microparticles. Optical microscopy and spectrophotometry were used to measure the purity of solution exchange qualitatively and quantitatively. Figure 3-5(a-f) show the upstream, downstream and outlet channels of the device under the microscope and their normalized gray intensity plots, along assessment lines AB, as reported in the previous chapter on Dean flow velocity. A higher gray value corresponds to a brighter region of DI water while a lower gray intensity shows darker areas with trypan blue. As seen, two clearly distinct phases were formed at the inlet (Figure 3-5(a-b)). The counter rotating vortices formed in the lateral direction of the channel caused the fluids to recirculate and switch positions near the outlet (Figure 3-5c). The width of the DI water region decreased slightly because of the minor mixing of trypan blue with DI water in Dean vortices (Figure 3-5d). The outlet channels were positioned in a way that the pure buffer was collected from the inner outlet as depicted in Figure 3-5(e-f). Quantitative measurement of the purity was performed by spectrophotometric analysis of the collected samples. The absorbance values yielded a solution purity of 99.2% in the inner outlet of the device as demonstrated by the table in Figure 3-5g(i). Pictures of the carrier fluid including the particles with diameters of 4 µm and 11 µm is shown in Figure 3-5g(ii). The majority of the 11 µm particles got transferred to the clean buffer (Figure 3-5g(iii)) while 4 µm particles were trapped in the carrier fluid and were extracted from the outer outlet as desired (Figure 3-5g(v)).

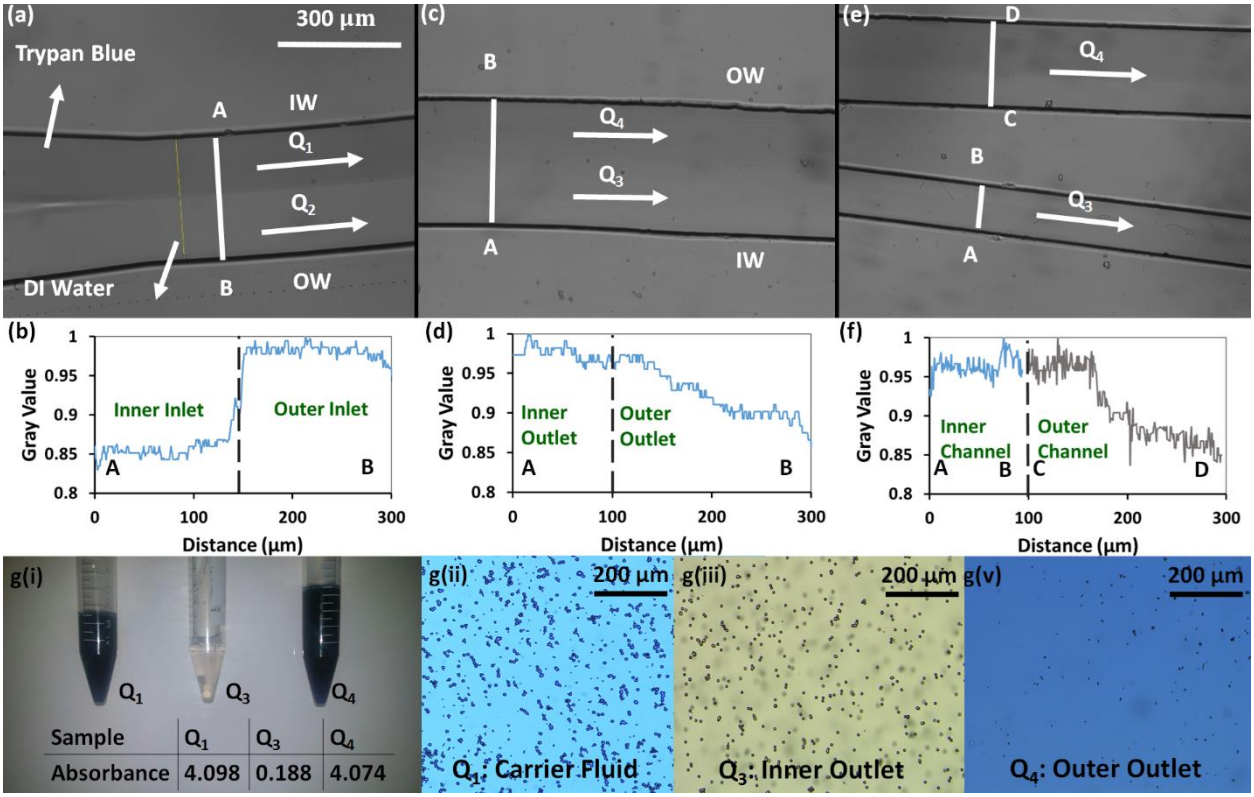

Figure 3-5. Quality of solution exchange and particle washing in the microfluidic centrifuge. (a-b) Upstream of the device (close to the inlet) and the normal gray intensity plot along line AB (Inner Wall: IW; Outer Wall: OW). (c-d) The outlet of the device where TB solution has been switched from the IW to the OW due to controlled Dean flow at Q1=Q2=1 mL.min^{-1}. The normal gray intensity value shows that water concentration is high at a 100 µm distance from the IW. However, from 100-200 µm, a mixed region was observed. The minimum gray intensity value was measured at 200-300 µm depicting the prevalent presence of TB close to the OW. (g(i)-g(v)) The initial solution consisting of 10% TB and microparticles of 4 and 11 µm size (Q1) and collected samples from the outlets (Q3 and Q4). The concentration of TB in the inner outlet was 0.8% (spectrophotometry table shown).

3.4.4 Solution Exchange and Separation of Surrogate Microparticles from Bacteria in the Device

After gaining parametric understanding of our device characteristics, its suitability for bacterial separation from target particles, mimicking cells and embryos, and their simultaneous solution exchange was investigated. We ran a solution of *E. coli* K12 ER2420/pACYC177 and 19 µm particles in LB broth (Miller) from the inner inlet (Figure 3-6a) and PBS as the target buffer from the outer inlet. The flow rate was similar to the case of DI water and trypan blue since the viscosity and density values were comparable with DI water. Optical microscopy of the collected samples confirmed that the

concentration of *E. coli* was significantly higher in the outer outlet while the majority of particles were collected from the inner outlet (Figure 3-6(b-c)). This is because *E. coli*, being smaller than 4 µm in effective diameter and possessing a very small R_f value, was in the Dean drag regime and got carried with the Dean flow to the outer outlet. However, 19 µm particles were focused close to the inner wall and mostly collected from the inner outlet. The collected samples were diluted and cultured on antibiotic-doped LB agar plates overnight to calculate the concentration of *E. coli* in the inner and outer outlets (Figure 3-6(d-e)). The number of colony forming units showed that 91±0.5% of *E. coli* remained in the LB broth solution and got separated from the 19 µm particles. This demonstrated the capability of our device in separating surrogate particles from bacterial contamination and washing them into a clean buffer for post sample preparation assays.

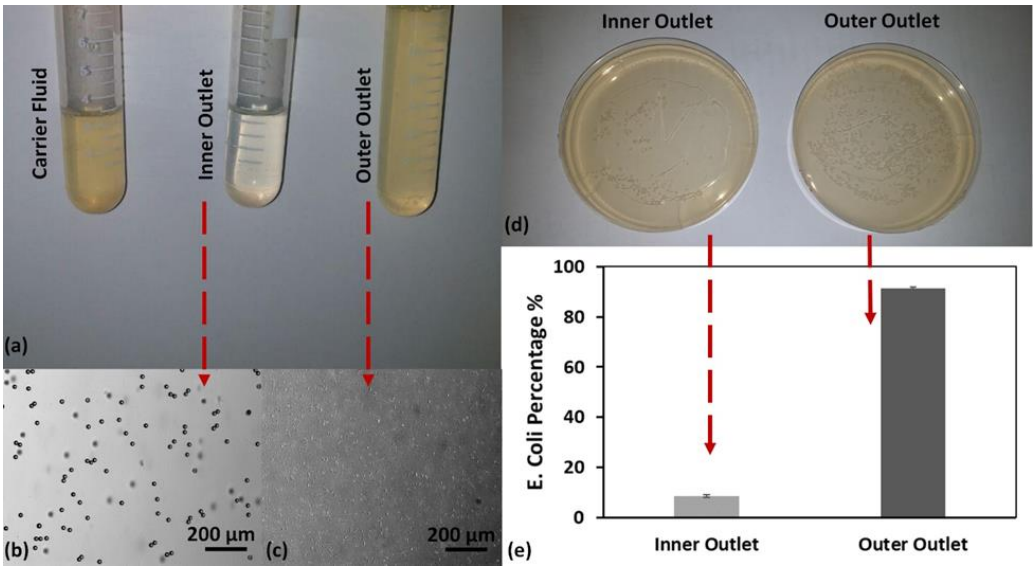

Figure 3-6. Continuous searation of bacteria from particles using the microfluidic centrifuge. (a) Initial suspension consisting of 19 µm particles and E. coli in LB broth and collected samples from the inner outlet and outer outlet. PBS that was initially in the outer traveled to the inner outlet and got replaced by LB broth. (b-c) Pictures of collected samples from the inner and outer outlet showing that 19 µm particles were focused close to the inner wall and got collected from the inner outlet while E. coli remained in its carrier solution and traveled to the outer outlet. (d) Pictures of cultured E. coli that was collected from the inner and outer outlets (e) Column plot showing the percentage of the cultured colonies yielding a 91±0.5% presence of E. coli in the outer outlet.

3.5 Conclusion

In this chapter, we designed a microfluidic device for exchanging the solution of microparticles, mimicking target cells or embryos, from a bacterial suspension to a clean buffer for applications that require processing high volumes of samples at high flow rates. We combined switching behavior of co-flows in curved microchannels at high velocities with inertial focusing of microparticles to achieve solution exchange and bacterial separation at a flow rate of 1 $mL.min^{-1}$ and particle concentration of 10^6 $particle.mL^{-1}$. Our device proved competency by exchanging the solution of 11 µm and 19 µm particles with efficiencies as high as 86±2% and 93±0.7%, respectively. We also performed simultaneous separation of these particles from smaller 4 µm particles or *E. coli* bacteria in our device with purities as high as 96±2% for particle isolation and 91±0.5% for the bacterial experiments. The separated and washed particles were obtained in outlet solutions with less than 1% impurity. Our technique proved to be a powerful platform for designing solution exchangers for particles and bacterial cells at high flow rates and specific fluidic conditions. However, further investigation of the device is needed to show the suitability of the device for washing and separation of human/animal cells from a bacterial solution.

Chapter 4

Thesis Summary and Future Work

4.1 Thesis Summary

In this thesis, we developed a new platform for exchanging the solution of microparticles with the possibility of extension to processing cells and bacteria in biological samples. According to our literature survey, several gaps were found in the currently available techniques both in the active and passive devices. The concept in both methods is to keep the sample fluid and the target buffer streamlined and side-by-side in a channel while transferring target particles from the sample solution to the buffer using external energies or inertial forces. This results in low operational flow rates (<100 $\mu L.min^{-1}$) and the lack of ability to process large-volume samples (>3 mL) with sufficient efficiencies (>90%).

We addressed the abovementioned technological shortcomings by manipulating both fluids and particles in a curved microchannel to make the solution exchange possible. Fluid manipulation was achieved by fundamental characterization of the secondary Dean flows of two liquids co-flown in a curved microchannel. The average velocity of Dean flow vortices (Dean velocity) was defined as the deterministic parameter that enables estimating the location of switching for the two liquids. Thus, upon a series of experimental and numerical parametric studies, a comprehensive correlation was derived for the

average Dean velocity incorporating the effects of hydraulic diameter, width and height of the channel, and viscosity of the fluids. Next, the forces that particles experience in a curved channel were identified, i.e. inertial and Dean drag forces, and studied. Two regimes of focusing were defined based on the ratio of these forces. The magnitudes of inertial force and Dean drag were calculated at Q= 1 $mL.min^{-1}$ and particles with various diameters were selected for analytical and experimental investigations. A device was then designed based on the derived formula for Dean velocity that guaranteed fluid switching at 1 $mL.min^{-1}$. The designed device was tested with the particles and simultaneous solution exchange of 11 µm particles and separation from 4 µm was reported with solution purity of 99.2% and separation efficiency of 95%. The biological application of the device was then shown by replacing the 4 µm with *E. coli* and 11 µm with 19 µm particles as cell surrogates. The results revealed that 91.5±0.5% of the bacteria got separated from the particles in our solution exchange microfluidic device.

4.2 Future Work

In this thesis, we studied the switching behavior of two Newtonian fluids in a curved microfluidic channel. The results were then used to design a solution exchanger device for testing with particles in the range of 4-22 µm. Based on the perception attained in our experiments, the following ideas are recommended for further investigations.

1- We have shown in chapter 2 that viscosity directly affects the average Dean velocity (V_{De}). However, we did not study the behavior of non-Newtonian fluids in a curved microchannel. Shear thickening and shear thinning fluids can be used for more in-depth investigation of the effect of non-Newtonian fluids on V_{De}. Another

direction may be co-flowing fluids with different viscosities in the channel to investigate their recirculation behavior as in some applications, target cells must be extracted from non-Newtonian fluids like blood and suspended in Newtonian buffers like PBS.

2- The inertial focusing in curved microchannels is not elaborated as much as straight channels. The interplay between the inertial force and Dean drag force can be studied on-chip by adding an expansion region at the end of the curved channel. The expansion region decreases the velocity of the particles and makes it feasible to quantify the focusing location of the particles under a microscope instead of off-chip counting. By measuring the focusing location at different flow rates in devices with various dimensions and radii of curvatures, the exact role of Dean drag and inertial forces can be found.

3- Our solution exchanger can be further developed by adding a reaction region to the device to completely mimic a biological process including reaction and washing steps. A spiral channel placed before the curved channel can serve as the reaction unit where two reagents are brought into contact and mixed by Dean flow. Reaction between two reagents normally requires more time compared to washing. The length of the spiral channel is larger than the curved section thus giving the reagents the time required for reaction while passing through the spiral. A clean buffer can be merged to the main stream after the spiral channel to transfer the analytes to the clean buffer in the curved channel after the reaction.

4- *Caenorhabditis elegans* (*C. elegans*) is a nematode that is of high interest to researchers as a disease model organism. The process of growing synchronized-

age *C. elegans* requires dissolving the body of the adult worms in bleach to release the eggs and multiple steps of centrifuging the eggs and washing with a clean buffer. This process is time consuming and can be damaging to the eggs if bleach exposure is not controlled in terms of time and concentration. Our device can be used as a means to wash the *C. elegans* eggs in one run. Therefore, the time required for solution exchange of the eggs reduces in our device while the purity of the solution exchange remains high (99.2%)

5- The larger particles in the experiments can be replaced with Eukaryotic cells for transferring them from the growth media to a clean buffer to investigate the effect of solution exchanger on vitality of the cells. The effect of deformability of the cells on focusing needs to be investigated in this case.

6- We hypothesized that the transition between Dean drag regime and inertial force regime is not abrupt as shown in Figure 3-2. There might be a transition regime through which the inertial force slightly prevails over the Dean drag. The boundaries of this transition region can be identified in our device by testing particles with various sizes between 4µm and 11µm. Upon defining the transition region, active sources of energy (such as magnetic force) can be added to the device to help the inertial force to focus the particles near the inner wall and overcome the Dean drag.

7- A platform for designing custom solution exchangers for any particle/cell diameter and flow rate can be prepared by performing solution exchange with various target sizes in devices with different geometrical parameters such as radius of curvature and width/height.

Bibliography

1 S. Schumacher, J. Nestler, T. Otto, M. Wegener, E. Ehrentreich-Förster, D. Michel, K. Wunderlich, S. Palzer, K. Sohn, A. Weber, M. Burgard, A. Grzesiak, A. Teichert, A. Brandenburg, B. Koger, J. Albers, E. Nebling and F. F. Bier, *Lab Chip*, 2012, **12**, 464–473.

2 I. M. Lazar and B. L. Karger, *Anal. Chem.*, 2002, **74**, 6259–6268.

3 L. M. Fu, R. J. Yang, G. B. Lee and Y. J. Pan, *Electrophoresis*, 2003, **24**, 3026–3032.

4 Y. Jiang, S. Zou and X. Cao, *Anal. Methods*, 2016, **8**.

5 W. Lee, D. Kwon, W. Choi, G. Y. Jung and S. Jeon, *Sci. Rep.*, 2015, **5**, 7717.

6 J. Kim, M. Johnson, P. Hill and B. K. Gale, *Integr. Biol.*, 2009, **1**, 574.

7 S. Kim, J. De Jonghe, A. B. Kulesa, D. Feldman, T. Vatanen, R. P. Bhattacharyya, B. Berdy, J. Gomez, J. Nolan, S. Epstein and P. C. Blainey, *Nat. Commun.*, 2017, **8**, 13919.

8 T. Nguyen, R. Pei, D. W. Landry, M. N. Stojanovic and Q. Lin, in *Sensors and Actuators, B: Chemical*, 2011, vol. 154, pp. 59–66.

9 N. Nivedita, N. Garg, A. P. Lee, I. Papautsky, D. T. Miyamoto, B. A. Waltman, S. M. Rothenberg, A. M. Shah, M. E. Smas, G. K. Korir, F. P. F. Jr., A. J. Gilman, J. B. Lord, D. Winokur, S. Springer, D. Irimia, S. Nagrath, L. V. Sequist, R. J. Lee, K. J. Isselbacher, S. Maheswaran, D. A. Haber and M. Toner, *Analyst*, 2017, **107**, 18392–18397.

10 J. Y. Zhang, J. Do, W. R. Premasiri, L. D. Ziegler and C. M. Klapperich, *Lab Chip*,

2010, **10**, 3265.

11 V. Kumar and P. Rezai, *Biomed. Microdevices*, 2017, **19**.

12 V. Kumar and P. Rezai, *Microfluid. Nanofluidics*, 2017, **21**.

13 M. Yu, Q. Wang, J. E. Patterson and A. T. Woolley, *Anal. Chem.*, 2011, **83**, 3541–3547.

14 B. Kim, J. K. Lee and S. Choi, *BioChip J.*, 2016, **10**, 81–87.

15 J. S. Dudani, D. R. Gossett, H. T. K. Tse, R. J. Lamm, R. P. Kulkarni and D. Di Carlo, *Biomicrofluidics*, 2015, **9**, 1–9.

16 S. S. H. Tsai, J. S. Wexler, J. Wan and H. A. Stone, *Appl. Phys. Lett.*, 2011, **99**.

17 J. J. Hawkes, R. W. Barber, D. R. Emerson and W. T. Coakley, *Lab Chip*, 2004, **4**, 446.

18 F. Petersson, A. Nilsson, H. Jönsson and T. Laurell, *Anal. Chem.*, 2005, **77**, 1216–1221.

19 S. Li, L. Ren, P. H. Huang, X. Yao, R. A. Cuento, J. P. McCoy, C. E. Cameron, S. J. Levine and T. J. Huang, *Anal. Chem.*, 2016, **88**, 5655–5661.

20 P. Augustsson, J. Persson, S. Ekström, M. Ohlin and T. Laurell, *Lab Chip*, 2009, **9**, 810–818.

21 S. Li, X. Ding, Z. Mao, Y. Chen, N. Nama, F. Guo, P. Li, L. Wang, C. E. Cameron and T. J. Huang, *Lab Chip*, 2015, **15**, 331–338.

22 S. a Peyman, A. Iles and N. Pamme, *Chem. Commun. (Camb).*, 2008, 1220–2.

23 S. A. Peyman, A. Iles and N. Pamme, *Lab Chip*, 2009, **9**, 3110.

24 M. Vojtisek, A. Iles and N. Pamme, *Biosens. Bioelectron.*, 2010, **25**, 2172–2176.

25 M. D. Tarn, R. F. Fakhrullin, V. N. Paunov and N. Pamme, *Mater. Lett.*, 2013, **95**,

182–185.

26 B.-U. Moon, N. Hakimi, D. K. Hwang and S. S. H. Tsai, *Biomicrofluidics*, 2014, **8**, 52103.

27 B. J. Kirby, *Micro-and nanoscale fluid mechanics: transport in microfluidic devices*, Cambridge University Press, 2010.

28 H.-C. Chang and L. Y. Yeo, 2010.

29 R. Diaz and S. Payen, 2008.

30 H. Morgan and N. G. Green, *AC electrokinetics: colloids and nanoparticles*, 2002, vol. 2.

31 R. Tornay, T. Braschler, N. Demierre, B. Steitz, A. Finka, H. Hofmann, J. A. Hubbell and P. Renaud, *Lab Chip*, 2008, **8**, 267–273.

32 S. Park, Y. Zhang, T.-H. Wang and S. Yang, *Lab Chip*, 2011, **11**, 2893.

33 J. M. Martel and M. Toner, *Annu. Rev. Biomed. Eng.*, 2014, **16**, 371–96.

34 J. M. Martel and M. Toner, *Sci. Rep.*, 2013, **3**, 1–8.

35 D. R. Gossett, H. T. K. Tse, J. S. Dudani, K. Goda, T. A. Woods, S. W. Graves and D. Di Carlo, *Small*, 2012, **8**, 2757–2764.

36 E. Sollier, D. E. Go, J. Che, D. R. Gossett, S. O'Byrne, W. M. Weaver, N. Kummer, M. Rettig, J. Goldman, N. Nickols, S. McCloskey, R. P. Kulkarni and D. Di Carlo, *Lab Chip*, 2014, **14**, 63–77.

37 B. Ha, J. Park, G. Destgeer, J. H. Jung and H. J. Sung, *Anal. Chem.*, 2016, **88**, 4205–4210.

38 N.-N. Deng, W. Wang, X.-J. Ju, R. Xie and L.-Y. Chu, *Lab Chip*, 2016, **16**, 4326–4332.

39 A. Mortari and L. Lorenzelli, *Biosens. Bioelectron.*, 2014, **60**, 8–21.

40 S. S. Kuntaegowdanahalli, A. A. S. Bhagat, G. Kumar and I. Papautsky, *Lab Chip*, 2009, **9**, 2973–2980.

41 J. Zhou and I. Papautsky, *Lab Chip*, 2013, **13**, 1121–1132.

42 H. W. Hou, M. E. Warkiani, B. L. Khoo, Z. R. Li, R. A. Soo, D. S.-W. Tan, W.-T. Lim, J. Han, A. A. S. Bhagat and C. T. Lim, *Sci. Rep.*, 2013, **3**.

43 J. Sun, M. Li, C. Liu, Y. Zhang, D. Liu, W. Liu, G. Hu and X. Jiang, *Lab Chip*, 2012, **12**, 3952–3960.

44 Z. Wu, B. Willing, J. Bjerketorp, J. K. Jansson and K. Hjort, *Lab Chip*, 2009, **9**, 1193–1199.

45 A. P. Sudarsan and V. M. Ugaz, *Lab Chip*, 2006, **6**, 74–82.

46 A. Alam and K.-Y. Kim, *Chem. Eng. J.*, 2012, **181**, 708–716.

47 M. E. Warkiani, A. Kah Ping Tay, G. Guan and J. Han, *Sci. Rep.*, 2015, 1–10.

48 D. Di Carlo, D. Irimia, R. G. Tompkins and M. Toner, *Proc. Natl. Acad. Sci.*, 2007, **104**, 18892–18897.

49 A. Russom, A. K. Gupta, S. Nagrath, D. Di Carlo, J. F. Edd and M. Toner, *New J. Phys.*, 2009, **11**, 0–9.

50 D. R. Gossett and D. Di Carlo, *Anal. Chem.*, 2009, **81**, 8459–8465.

51 S. S. Kuntaegowdanahalli, A. A. S. Bhagat, G. Kumar and I. Papautsky, *Lab Chip*, 2009, **9**, 2973–2980.

52 J. M. Martel and M. Toner, *Annu. Rev. Biomed. Eng.*, 2014, **16**, 371–396.

53 N. Nivedita, P. Ligrani and I. Papautsky, *Nat. Publ. Gr.*, 2017, 1–10.

54 A. Gigras and S. Pushpavanam, *Microfluid. Nanofluidics*, 2008, **5**, 89–99.

55 A. P. Sudarsan and V. M. Ugaz, *Proc. Natl. Acad. Sci. U. S. A.*, 2006, **103**, 7228–7233.

56 Y. Yamaguchi, F. Takagi, T. Watari, K. Yamashita, H. Nakamura, H. Shimizu and H. Maeda, *Chem. Eng. J.*, 2004, **101**, 367–372.

57 A. A. S. Bhagat, S. S. Kuntaegowdanahalli and I. Papautsky, *Lab Chip*, 2008, **8**, 1906.

58 J. M. Ottino and S. Wiggins, *Philos. Trans. Math. Phys. Eng. Sci.*, 2004, **362**, 923–935.

59 X. L. Mao, J. R. Waldeisen, B. K. Juluri and T. J. Huang, *Lab Chip*, 2007, **7**, 1303–1308.

60 D. H. Yoon, J. B. Ha, Y. K. Bahk, T. Arakawa, S. Shoji and J. S. Go, *Lab Chip*, 2009, **9**, 87–90.

61 K. Brun and R. Kurz, *Int. J. Rotating Mach.*, 2005, **2005**, 45–52.

62 P. Kulkarni, P. A. Baron and K. Willeke, *Aerosol Measurement: Principles, Techniques, and Applications: Third Edition*, 2011.

63 D. N. Ku, *Annu. Rev. Fluid Mech.*, 1997, **29**, 399–434.

64 S. Wang and K. Vafai, *Ann. Biomed. Eng.*, 2015, **43**, 1571–1584.

65 M. Motomiya and T. Karino, *Stroke*, 1984, **15**, 50–56.

66 J. M. Martel and M. Toner, *Phys. Fluids*, 2012, **24**.

67 S. Ookawara, R. Higashi, D. Street and K. Ogawa, *Chem. Eng. J.*, 2004, **101**, 171–178.

68 S. A. Berger, L. Talbot and L. S. Yao, *Annu. Rev. Fluid Mech.*, 1983, **15**, 461–512.

69 D. Doorly and S. Sherwin, *Cardiovasc. Math.*, 2009, 177–209.

70 M. Norouzi and N. Biglari, *Phys. Fluids*, 2013, **25**.

71 S. Yanase, N. Goto and K. Yamamoto, *Fluid Dyn. Res.*, 1989, **5**, 191–201.

72 M. Norouzi, M. H. Sedaghat and M. M. Shahmardan, *J. Nonnewton. Fluid Mech.*, 2014, **204**, 62–71.

73 M. Norouzi, B. Z. Vamerzani, M. Davoodi, N. Biglari and M. M. Shahmardan, *Rheol. Acta*, 2015, **54**, 391–402.

74 M. Norouzi, M. H. Kayhani, C. Shu and M. R. H. Nobari, *J. Nonnewton. Fluid Mech.*, 2010, **165**, 323–339.

75 J. Zhang, B. Zhang and J. Jü, *Int. J. Heat fluid flow*, 2001, **22**, 583–592.

76 P. M. Ligrani and R. D. Niver, *Phys. fluids*, 1988, **31**, 3605–3617.

77 B. Bara, K. Nandakumar and J. H. Masliyah, *J. Fluid Mech.*, 1992, **244**, 339–376.

78 K. Yamamoto, X. Wu, K. Nozaki and Y. Hayamizu, *Fluid Dyn. Res.*, 2006, **38**, 1–18.

79 S. Kim and S. J. Lee, *Exp. Fluids*, 2009, **46**, 255–264.

80 D. Di Carlo, *Lab Chip*, 2009, **9**, 3038–3046.

81 Google Patents, US4346164 A, 1982.

82 Y. Xia and G. M. Whitesides, *Annu. Rev. Mater. Sci.*, 1998, **28**, 153–184.

83 N.-S. Cheng, *Ind. Eng. Chem. Res.*, 2008, **47**, 3285–3288.

84 Y. K. Suh and S. Kang, *Micromachines*, 2010, **1**, 82–111.

85 G. Guan, L. Wu, A. A. Bhagat, Z. Li, P. C. Y. Chen, S. Chao, C. J. Ong and J. Han, *Sci. Rep.*, 2013, **3**, 1475.

86 N. R. Draper and H. Smith, *Technometrics*, 1998, **47**, 706.

87 D. C. Duffy, J. C. McDonald, O. J. A. Schueller and G. M. Whitesides, *Anal. Chem.*, 1998, **70**, 4974–4984.